Investigation of Networked SSHI Configurations for Plate-Based Piezoelectric Energy Harvesting

by

Engin Tarhan

A Thesis Submitted to the
Graduate School of Sciences and Engineering
in Partial Fulfillment of the Requirements for
the Degree of

Master of Science

in

Mechanical Engineering

KOÇ
ÜNİVERSİTESİ

August 16, 2023

Investigation of Networked SSHI Configurations for Plate-Based Piezoelectric Energy Harvesting

Koç University

Graduate School of Sciences and Engineering

This is to certify that I have examined this copy of a master's thesis by

Engin Tarhan

and have found that it is complete and satisfactory in all respects,

and that any and all revisions required by the final

examining committee have been made.

Committee Members:

____

Ipek Basdogan, Ph.D. (Advisor)

____

Amirreza Aghakhani, Ph.D.

____

Bekir Bediz, Ph.D.

Date: ______________________________

Dedicated to my family…

ABSTRACT

Investigation of Networked SSHI Configurations for Plate-Based Piezoelectric Energy Harvesting

Engin Tarhan
Master of Science in Mechanical Engineering
August 16, 2023

Vibration-based energy harvesting has received significant interest over the past two decades to generate electrical power to be used in small electrical devices and components mostly powered with conventional batteries to reduce maintenance cost and eliminate battery disposal. Among the existing transduction mechanisms, piezoelectric transducers are in the interest of the researchers as they have large power densities. In the majority of the studies about harvesting applications, the piezoelectric energy harvesters are in the form of cantilevered beams, with one or two layers of piezoelectric materials, which are known as unimorph configuration and bimorph configuration, respectively. As an alternative to the cantilever beam energy harvesters, patch-based piezoelectric energy harvesters are more efficient and easier to implement on plate-like structures to convert the vibrational energy of the host structure to electrical energy. Piezo-patch energy harvesters attached to plate-like structures can be used to extract multimodal vibrational energy in automotive, aerospace, and marine applications. The alternating current obtained from energy harvesting should be transformed into a more stable (DC) form for practical applications. For most of these transformations, a full wave standard AC-DC rectifier circuits are used. To improve the output power, researchers have studied several circuits, including synchronized switch harvesting on inductor (SSHI) circuits. For each piezo patch, SSHI circuits can boost the harvested power compared to standard rectifier harvesting circuits. However, the effect of using different configurations of the SSHI networks for multiple piezo patches on plate structures have not yet been understood. This study aims to assess the performance of the networked SSHI configurations compared to networked rectifier configurations and investigate the optimum configurations for energy harvesting purposes. In this study, three piezo patches are bonded to an aluminum host plate and connected to single and/or multiple energy harvesting circuits. The electromechanical system's equivalent circuit model (ECM) is developed from the experimentally validated analytical model and utilized in an electronic circuit simulation software LTspice. Four different case studies of single/ multiple rectifiers and SSHI circuits are considered. The first two cases include a single rectifier/SSHI circuit, while the other two include separate rectifier/SSHI circuits for each patch. The performances of each configuration are evaluated under harmonic excitation in terms of peak power outputs, and the optimal load resistances are obtained for each configuration. Based on the experimental findings, the best configuration is determined and verified by the ECM results. The results show that by using respective SSHIs, the power output can be improved by preventing charge cancellation despite the cost of increased diode loss. This study contributes to our understanding of optimal energy harvesting techniques by investigating the effectiveness of networked SSHI configurations for multiple piezo patches on plate structures.

Keywords: Networked SSHI, Piezoelectric, Multimodal Energy Harvesting, Equivalent Circuit Model, Plate

ÖZETÇE

Plaka Tabanlı Piezoelektrik Enerji Hasatlamak için Ağ Bağlantılı SSHI Konfigürasyonlarının İncelenmesi

Engin Tarhan

Makine Mühendisliği, Yüksek Lisans

16 Ağustos 2023

Titreşime dayalı enerji hasadı, bakım maliyetini azaltmak ve pilin atılmasını ortadan kaldırmak için çoğunlukla geleneksel pillerle çalışan küçük elektrikli cihazlarda ve bileşenlerde kullanılacak elektrik enerjisi üretmek için son yirmi yılda büyük ilgi görmüştür. Mevcut transdüksiyon mekanizmaları arasında piezoelektrik dönüştürücüler, büyük güç yoğunluklarına sahip oldukları için araştırmacıların ilgi alanına girmektedir. Piezoelektrik enerji hasadı ile ilgili çalışmaların çoğunda, piezoelektrik enerji hasatlayıcılar, basit yapılarından dolayı, sırasıyla unimorf konfigürasyon ve bimorf konfigürasyon olarak bilinen sırasıyla bir veya iki piezoelektrik malzeme tabakası ile konsol kirişler şeklindedir. Konsol kirişli enerji hasatlayıcılara bir alternatif olarak, yama tabanlı piezoelektrik enerji hasatlayıcıların, ana yapının titreşim enerjisini elektrik enerjisine dönüştürmek için plaka benzeri yapılar üzerinde uygulanması daha verimli ve daha kolaydır. Plaka benzeri yapılara bağlı piezo-yama enerji hasatlayıcılar, otomotiv, havacılık ve denizcilik uygulamalarında çok modlu titreşim enerjisini çıkarmak için kullanılabilir. Enerji hasadından elde edilen alternatif akım, pratik uygulamalar için daha kararlı (DC) bir forma dönüştürülmelidir. Bu dönüşümlerin çoğu için tam dalga standart AC-DC doğrultucu devreleri kullanılır. Çıkış gücünü artırmak için araştırmacılar, indüktör üzerinde senkronize anahtar hasatlayıcı (SSHI) da dahil olmak üzere çeşitli devreler üzerinde çalıştılar. Her piezo yaması için, SSHI devreleri, standart doğrultucu toplama devrelerine kıyasla toplanan gücü artırabilir. Bununla birlikte, SSHI ağının farklı konfigürasyonlarını çoklu piezo yamalar için kullanmanın plaka yapıları üzerindeki etkisi henüz anlaşılamamıştır. Bu çalışma, ağa bağlı SSHI konfigürasyonlarının performansını ağa bağlı doğrultucu konfigürasyonlarına kıyasla değerlendirmeyi ve enerji hasadı uygulamaları için optimum konfigürasyonları araştırmayı amaçlamaktadır. Bu çalışmada, üç piezo-yaması bir alüminyum ana plakaya yapıştırılmış ve tekli ve/veya çoklu enerji hasatlama devrelerine bağlanmıştır. Elektromekanik sistemin eşdeğer devre modeli (ECM), deneysel olarak onaylanmış analitik modelden geliştirilmiştir ve bir elektronik devre simülasyon yazılımı olan LTspice'da kullanılmıştır. Tekli/çoklu doğrultucular ve SSHI devreleriyle ilgili dört farklı konfigürasyon çalışması ele alınmıştır. İlk iki durum tek bir doğrultucu/SSHI devresini içerirken, diğer ikisi her yama için ayrı doğrultucu/SSHI devrelerini içermektedir. Her konfigürasyonun performansı, harmonik uyarım altında tepe güç çıkışları açısından değerlendirilmiştir ve her konfigürasyon için optimum yük dirençleri elde edilmiştir. Deneysel bulgulara dayanarak, en iyi konfigürasyon belirlenmiştir ve deneysel sonuçlar simülasyon sonuçları tarafından doğrulanmıştır. Sonuçlar, ilgili SSHI'ları kullanarak, artan diyot kaybına rağmen yük kaybını önleyerek güç çıkışının iyileştirilebileceğini göstermektedir. Bu çalışma, plaka yapıları üzerindeki çoklu piezo-yamaları için ağ bağlantılı SSHI konfigürasyonlarının etkinliğini araştırarak optimum enerji hasatlama tekniklerini anlamamıza katkıda bulunuyor.

Anahtar Kelimeler: Ağa Bağlı SSHI, Piezoelektrik, Multimodal Enerji Hasatlama, Eşdeğer Devre Modeli, Plaka

ACKNOWLEDGEMENTS

First and foremost, would like to express my sincere gratitude to my advisor Prof. Dr. Ipek Basdogan, for giving me the chance to be a member of the Vibration and Acoustics Laboratory, creating an instructive, supportive, and comfortable research environment. I am grateful for her patience, guidance, and unwavering support during my research years at Koç University. Her supervision and professional perspective on research have always helped me overcome the obstacles I encountered throughout this my master studies.

Beside my advisor, I am grateful to Assist. Prof. Amirreza Aghakhani for his guidance, valuable comments, encouragement, and collaboration. His directions and suggestions were very crucial for my research.

I am also more than thankful to Assist. Prof. Bekir Bediz for his thorough review of my work and showing delicacy to attend my thesis defense.

I am very thankful to my dear friends and lab mates Seyed Morteza Hoseyni and Mehmet Ramazan Şimşek for providing very valuable and insightful discussions to throughout my research. Their commendable help during my tough times opened the path for me to finish my thesis successfully.

Last but not least, I would like to thank my parents, my brother and my dear friend Alex for supporting me in every way that is possible.

TABLE OF CONTENTS

LIST OF TABLES xi

LIST OF FIGURES xii

NOMENCLATURE xiv

Chapter 1 1

INTRODUCTION 1

1.1. Vibrational Energy Harvesting Using Piezoelectricity 1

1.2. Review of the Existing Mathematical Models for Piezoelectric Energy Harvesters 6

1.3. Review of the Existing Equivalent Circuit Models for Piezoelectric Energy Harvesters Connected to Nonlinear Circuits 8

1.4. Thesis Outline and Layout 9

Chapter 2 10

THE DISTRIBUTED PARAMETER MODEL AND THE EQUIVALENT CIRCUIT MODELING OF MULTIPLE PIEZO-PATCHES ON A THIN-PLATE 10

2.1. Distributed Parameter Model of Multiple Piezo-patches Attached on A Thin-Plate 10

2.1.1. Electromechanical equations for series configuration 11

2.1.2. Electromechanical equations for parallel configuration 13

2.2. Equivalent Circuit Modeling Overview 14

2.3. Equivalent Circuit Analogy 15

2.4. Equivalent Circuit Model of Multiple Piezo-patches Attached on a Thin-plate 17

Chapter 3 19

THE NETWORKED CONFIGURATIONS AND THE EXPERIMENTAL SETUP 19

3.1. SSHI Circuit Schematic and The Networked Configurations 19

3.2. The Experimental Setup... 22

3.3. Mode Shapes of The Structure 24

Chapter 4.. 26

EQUIVALENT CIRCUIT MODEL VERIFICATION AND THE HARVESTING PERFORMANCE ANALYSES OF THE NETWORKED CONFIGURATIONS. 26

4.1. AC input – AC output verifications 26

4.2. AC input – DC output verifications 28

Chapter 5.. 34

SUMMARY, CONCLUSION AND FUTURE WORK... 34

BIBLIOGRAPHY.. 37

LIST OF TABLES

Table 2.1. Analogy of mechanical and electrical systems. 17

Table 2.2. Equivalent Circuit Modeling Parameters and Their Mechanical Counterparts 18

Table 3.1. SSHI Circuit Elements. 20

Table 3.2. Geometric and material properties of the host plate and the piezoceramics. 24

Table 4.1. Improvement/deterioration of the experimental peak power outputs after using networked SSHI circuit instead of networked rectifier circuit. 33

Table 4.2. Experimental peak power outputs of the four networked SSHI configurations. 33

LIST OF FIGURES

Figure 2.1. Multiple piezo-patch energy harvesters attached on a thin plate integrated with an SSHI circuit: (a) Series configuration (b) Parallel configuration. 11

Figure 2.2. Electrical schematic of series connection of MPEHs integrated with an SSHI circuit. 12

Figure 2.3. Electrical schematic of parallel connection of MPEHs integrated with an SSHI circuit. 14

Figure 2.4. Mechanical (a) and electrical (b) representation of a system. 16

Figure 2.5. Equivalent circuit model of the plate coupled with a piezo-patch, where each branch represents a mode (m×n modes in total). 18

Figure 3.1. SSHI Circuit Schematic.. 19

Figure 3.2. SSHI circuit switching device in LTspice. 20

Figure 3.3. The circuit models for all configurations and the expansion of $Z_{circuit}$. (a) Configuration A: Multiple series patches – single rectifier/SSHI. (b) configuration B: Multiple parallel patches – single SSHI. (c) Configuration C: Multiple patches – multiple series rectifiers/SSHIs. (d) Configuration D: Multiple patches – multiple parallel rectifiers/SSHIs. (e) SSHI and rectifier circuit components. 21

Figure 3.4. Experimental setup: (a) PZT-1, (b) PZT-2, (c) PZT-3, (d) aluminum host plate, (e) clamping frames, (f) shaker with a force transducer, (g) SSHI circuits, (h) signal generator, (i) data acquisition unit and (j) laser vibrometer. 23

Figure 3.5. Normalized strain mode shapes of the structure for the first five modes..... 25

Figure 4.1. Parameters of the signal generator for the AC input-AC output experiments. 26

Figure 4.2. Comparison of experimental and numerical model for the AC input- AC output case. Three piezo-patches are connected in series (a) and parallel (b) configurations, and a load resistance of 1MΩ is connected to the output of the configurations. 27

Figure 4.3. LTspice and experiment results presenting the variations of voltage FRFs (V/N) of the four different configurations for networked SSHI; configuration A: LTspice (a) and experiment (b); configuration B: LTspice (c) and experiment (d); configuration C: LTspice (e) and experiment (f) and configuration D: LTspice (g) and experiment (h) for thirteen load resistances ranging from 1kΩ to 1MΩ. 29

Figure 4.4. Comparison of peak power outputs of the four configurations of networked rectifier and networked SSHI versus varying resistances from 1 kΩ to 1 MΩ for the first five modes; both experimental and numerical results. 32

NOMENCLATURE

a	Length of the plate
b	Width of the plate
C	Equivalent capacitance
C_p	Internal capacitance of piezo-patch
d^{31}	Piezoelectric constant
$\bar{e}_{31}$	Effective piezoelectric constant
f	Transverse point force
h_p	Thickness of the piezoceramic harvester
h_{pc}	Distance of the center layer of the piezo-patch from the reference surface
h_s	Thickness of the plate
i	Equivalent electrical current
i_c	Current passing into the SSHI circuit
L	Equivalent inductance
l_p	Length of the piezo-patch
$n_{\bar{p}}$	Number of piezoceramic patches
p	Subscript notation for piezoceramic properties
R	Equivalent resistance
R_l	Resistive load
s	Subscript notation for plate properties
V	Equivalent voltage source
v	Electrode voltage across the external resistive load
w_p	Width of the piezo-patch
$x_{k,1}$	x-coordinate of the left edge of kth piezo-patch
$x_{k,2}$	x-coordinate of the right edge of kth piezo-patch

x_0	x-coordinate of the applied point force
$y_{k,1}$	y-coordinate of the bottom edge of kth piezo-patch
$y_{k,2}$	y-coordinate of the upper edge of kth piezo-patch
y_0	y-coordinate of the applied point force
$\bar{\varepsilon}$	Permittivity term
$\bar{\varepsilon}_{33}^{S}$	Permittivity constant
ζ_{mn}	Modal damping ratio
θ	Electromechanical term
$\tilde{\theta}$	Electromechanical coupling term
ϕ	Mass normalized eigenfunction
ω_{mn}	Undamped natural frequency

(This page intentionally left blank)

Chapter 1

INTRODUCTION

1.1. Vibrational Energy Harvesting Using Piezoelectricity

Clean and renewable energy sources are the ultimate need of our planet as non-renewable natural energy sources are limited. Harvesting energy from ambient sources is a promising way to provide continuous energy supply. There are numerous forms of renewable energy, such as solar energy, geothermal energy, wind energy, hydro energy, vibrational energy, tidal energy, and biomass energy. Among these resources, vibrational energy is the most ubiquitous and accessible one, as it relies on movement in general and not limited to concentrated sources such as wind or sunlight [1].

In the past decade, vibration-based energy harvesting has received a great interest which mainly aims to generate electrical power to be used in small electrical devices and components which are mostly powered with conventional batteries. However, the development of conventional batteries is progressing quite slowly. One of the most popular conventional battery type Li-ion battery, for example was issued in the market more than 30 years ago. When comparing the advancement of technology, it is evident that the development of batteries has been insufficient to keep up with state-of-the-art technologies. This is primarily because the advancement in technology has led to increased power usage in electronics [2]. This excessive need of power of electronic devices causes reduction in battery life. Since these conventional batteries requires replacement, and they have certain lifetime, vibration-based energy harvesting became a good option to eliminate these conventional batteries as it enables self-powered systems [3].

Many researchers have focused on obtaining electrical power from vibrational energy sources in their studies to find an alternative to conventional batteries [2-6]. To convert vibrational energy to electrical energy, there are several methods used, which can be categorized by fundamental transducing principles and by smart materials. While electrostatic [4] and electromagnetic [5] are two examples of the well-known fundamental transducing principles, piezoelectric [3, 6], electroactive [7], magnetostrictive [8, 9], and metamaterials are examples of the transduction principles by smart materials. Among these, the key advantage of using piezoelectric materials for energy harvesting is that piezoelectric materials have large power densities, and they are easy to implement. Also, in piezoelectric energy harvesting, voltage outputs that are obtained can be readily used as they directly convert the applied strain energy to usable electrical energy in contrast to electromagnetic energy harvesting where post processing like voltage multiplication is necessary to use the output voltage [3].

Piezoelectric materials has an effect called piezoelectric effect to generate electrical energy when stress is applied [10], and they also have the ability to generate stress when an electric field is applied on. These two effects exist in a piezoelectric material at the same time, so they both need to be accounted in the applications.

The working principle of piezoelectric materials is that these materials are ionically bonded and contain both positive and negative ions and when the mechanical stress applied on these materials, electric dipole occurs as the positive and negative ions move. At this point, the anisotropic dielectric characteristic of these materials turns into charged materials. The negative and positive charges move to opposite sides of the crystal face, and these charges are collected by the metal plate to obtain a voltage output across the opposite crystal faces [11].

There are many factors affecting the performance of the energy harvester, and type of the piezoelectric material is one of them. Several piezoelectric materials are available as commercial products, but among these materials, piezoceramic lead zirconate titanate (PZT) is the most common one for energy harvesting purposes. Although its wide usage, PZT has certain limitations about the strain it can absorb since fatigue crack growth can take place in cyclic loadings due to its brittleness. As an alternative to PZT, polyvinylidene fluoride (PVDF) is also a widely used material and it has more flexibility inherently. The reason why PZT is more preferred compared to PVDF although PVDF has more flexibility is that PZT has much higher electromechanical coupling compared to PVDF, and the density of PZT is much higher. In a study conducted by Sodano et al. [12], three different piezoelectric materials, which are PZT, macro fiber composite (MFC), and quick pack (QP) actuator have been tested and compared. The deduction has been made that PZT is the most consistent and efficient one among all three materials, especially for the random vibrations.

In most of the studies about piezoelectric energy harvesting, the piezoelectric energy harvesters are in the form of cantilevered beams, and these harvesters come with one or two layers of piezoelectric materials which are known as unimorph configuration and bimorph configuration, respectively [3]. In these configurations, the harvester beams are mounted on a vibrating host plate. The alternating voltage is obtained across the electrodes, and this voltage is the result of the harmonic base motion of the host structure. Johnson et al. [13] designed an unimorph cantilever beam harvester. Sodano et al. [14], have studied on bimorph configuration of a cantilever beam and they developed a mathematical model for the energy generation. Jiang et al. [15] have studied the efficiency of the bimorph configuration and assessed the performance change based on physical and geometrical parameters. Roundy and Zhang [16] have studied tuning the harvesting device to obtain the same frequency as the ambient vibrations, to increase the efficiency of the energy harvesting.

Although the cantilever beam harvester configuration is the configuration that has been most deeply studied on in the literature, it has a significant drawback. The power generation severely drops for the off-resonance frequency values for this type of harvesters, and therefore they are not practical for harvesting the energy in a broadband form for the real-life applications where the excitation frequency varies [17]. This type of harvesters must be excited at the resonance frequencies to have at least a mediocre power generation. The tuning of the harvester can be made by attaching a mass at the end tip, but in some cases this application causes problems as it increases the weight of the harvester, and even cause mechanical failure [18].

As an alternative to the cantilever beam energy harvesters, patch-based piezoelectric energy harvesters are more efficient and easier to implement on plate-like structures to convert the vibrational energy of the host structure to electrical energy. Thin plate structures are widely used in many areas such as automotive, aerospace and marine, and the applicability of patch-based energy harvesters are advantageous compared to cantilever beam energy harvesters as larger number of vibration modes are observed for specific range of frequencies. As a result of this, a more broadband energy harvesting is achieved.

In most of the models of cantilever beam harvesters and plate harvesters, a resistive load is used to examine the power output. However, the situation is different when it comes to practical purposes like transferring the power to a storage capacitor. For practical purposes, the alternating current obtained from energy harvesting should be transformed to a more stable form. For this purpose, the alternating current (AC) is transformed to a steady rectified current, which is also referred as direct current (DC) with the help of a rectifier bridge. For most of these transformations, a full wave AC-DC rectifier is used. In addition to this AC-DC transformation, it is advantageous to use a smoothing capacitor to improve the performance where the smoothing capacitor acts as a DC-DC converter. Although the voltage regulation can be obtained by DC-DC converters, the output power is not satisfactory and would be better to be improved. For this purpose, Lefeuvre et al. [19] have developed a self-adaptive circuit named SECE, which stands for “synchronous electric charge extraction”. The SECE circuit is composed of a diode bridge that acts as a rectifier and a flyback converter that acts as a DC-DC converter which is activated when the voltage peaks and charges the battery or the storing capacitor. After the extraction of all the electric charge, the flyback converter gets deactivated, and this process is repeated. By this concept, approximately four times higher energy is harvested compared to the unsynchronized direct charging.

Guyomar et al. [20] and Badel et al. [21], have conducted studies on other methods to improve the efficiency. They focused on synchronizing the vibrations of the system and the electric charge extraction and named the circuit as the SSHI circuit, which stands for “synchronized switch harvesting on inductor”. The schematic of the circuit is that the switching device is connected to an inductor in series, and these two are integrated between the piezoelectric patch and the rectifier circuit in parallel configuration. The working principle of the SSHI circuit is the switching device gets triggered when the mechanical displacement of the harvester reaches an extremum which leads to the quasi-instantaneous inversion of the polarity of the piezoelectric element. By the repetition of this process, the voltage is improved [20, 22], up to 15 times higher compared to direct charging [18]. The studies show that SSHI circuit is a good choice mainly for weakly coupled piezoelectric harvesters. There are numerous studies focusing on especially the circuitry of the SSHI, and these studies are summarized by Chao [23]. Recently, Hoseyni, et al. [24] developed an analytical model based on equivalent impedance approach for a piezoelectric energy harvester integrated on a thin plate with a single SSHI circuit.

There are different types of SSHIs in the literature, where most of them are series-SSHIs (s-SSHI) and parallel-SSHIs (p-SSHI). In p-SSHI, the inductor and the switching device is connected in parallel between the piezoelectric generator and the rectifier. On the contrary, in s-SSHI, an inductor and a switching device is connected in series between the piezoelectric generator and the rectifier. In the literature, both series-SSHI and parallel-SSHI harvesting circuits are investigated. Shu et al. [25] made a comparison between p-SSHI and s-SSHI performances for weakly, averagely and strongly coupled systems. They determined that for weakly coupled systems although both s-SSHI and p-SSHI boosted the maximum power at a similar rate, the maximum power of the case where p-SSHI is used is slightly higher. For averagely electromechanically coupled systems, the power is not boosted in both configurations compared to standard interface, and lastly for strongly electromechanically coupled systems, while p-SSHI acts like a standard interface circuit at short circuit resonance, the s-SSHI acts similar to standard interface at open circuit resonance. Also, the authors deduced that the optimal electric load of p-SSHI and s-SSHI are inversely proportional to each other. Lien et al. [26] have proposed an improved analytical expression for s-SSHI which takes the phase-shift effect, and compared the results with the piezoelectric systems where standard interface or p-SSHI is used. As a result, they came up with the same conclusion as [25] and further concluded that although p-SSHI maintains its bandwidth improvement, s-SSHI might lose its improvement when the diode losses are considered. In another study, Lin et al. [27] have evaluated the performance of p-SSHI and s-SSHI circuits and found that the s-SSHI results in a wider bandwidth but a lower peak power.

Although there are some studies about evaluating the performance of the SSHI circuits [25], there are limited number of studies focusing on the networked configurations of the SSHI circuits. Wu et al. [28] have studied SSHI circuits on the improvement of vibration damping of a clamped steel plate. They have proposed two networks, which are synchronized switch damping by energy transfer (SSDT) and synchronized switch damping with diode (SSDD) and compared these networks' performances with synchronized switch damping on an inductor (SSDI) baseline. While SSDT relies on the principle of switching synchronized with the structure modal coordinates and obtaining a voltage inversion for damping, SSDD relies on the principle of orienting the energy flow by using the diode's one-way allowance of current. Both networks they proposed resulted in a better performance in terms of damping. Li et al.

[29] have studied network of the piezoelectric elements for energy harvesting purposes focusing on the first four modes. However, their study only involved numerical simulations conducted in Simulink, and the excitation was limited to pulse mode. But in pulse mode, the energy is distributed in several modes according to the structure's natural impulse response, and for different energy distributions, simply a harmonic force can be applied instead of a pulse excitation [28].

1.2. Review of the Existing Mathematical Models for Piezoelectric Energy Harvesters

The purpose of the mathematical models of piezoelectric energy harvesters is to predict the voltage output, thus power output, on the integrated resistive load and evaluate the conversion efficiency from mechanical to electrical energy. The piezoelectric energy harvesting problem has been investigated by researchers from mechanical field, electrical field, and materials field from different ways. There are numerous approaches in the literature that considers the modeling of the energy harvesters.

The first of these modeling approaches is the lumped-parameter modeling, which is a type of single degree-of-freedom (SDOF) model [3]. The first SDOF model proposed is composed of a mass, a spring and a damper and the problem is given as a base excitation problem. This model was acceptable for the situations that the inertial excitation is dominant compared to the damping of the external fluid. However, it was insufficient for the situations where the harvester is operating in fluids where the external damping of the fluid needs to be accounted like viscous fluids. In addition, this model was not valid for the micro-scale devices. In these cases, the damping is represented as the air damping coefficient and the viscous damping coefficient, distinctively. In their studies, Jeon et al. [30] and Fang et al. [31] have used the model of Williams and Yates [32], but this model was for certain electromagnetic transducers and this model does not hold for piezoelectric transduction as it assumes that the backward coupling (electrical damping) is linear and proportional to the velocity. duToit et al. [33] have modeled the backward coupling correctly, and they used the longitudinal vibrations (vibrations in 3-direction) rather than bending. Also, they achieved to observe the short circuit and the open circuit trends. Erturk and Inman have studied on improving the model of duToit, and they derived some correction factors for more accurate results [34]. In another study, Roundy et al. [17, 35]

presented a model for bimorph cantilever beam, where they did not take the distributed mass of the beam into account as they assumed the tip mass is significantly larger. This model had some defects as the distributed mass needs to be take accounted as it affects not only the natural frequencies of the harvester, but also the excitation force amplitude. Again, Erturk and Inman [34] have shared related correction factors in their study. The lumped-parameter models approach energy harvesting in a simpler perspective, and they provide a simple understanding to understand the harvesting concept. But even so, the lumped parameter models are not comprehensive and limited to predict the harvesting performance as they are restricted to o a single vibration mode. These models cannot capture the higher vibration modes; therefore, they are highly inaccurate for the higher frequencies.

Due to the inaccuracies of the lumped-parameter models, researchers have studied on several distributed-parameter models. One of these models is the Rayleigh-Ritz discretization which is an approximate representation of the distributed parameter system [36, 37]. The model reduces the number of mechanical degrees of freedom of the system from infinity to a finite number and although it requires more computational effort, it is preferable compared to lumped-parameter models as it’s more accurate.

In order to reduce the computational effort of Rayleigh-Ritz discretization, researchers have developed analytical models which are also stated as distributed parameter models [38-40]. The analytical models that are developed earlier are inaccurate and had some deficiencies. The reason is that they neglected the backward piezoelectric coupling, represented the base excitation as a forcing term although it is not a typical external load and ignored the modal expansion effects [41]. Erturk and Inman [42] have presented the exact analytical model for of a cantilevered piezoelectric energy harvester using Euler–Bernoulli beam assumptions.

Although there are many studies about the cantilevered beam energy harvesting, the studies about the piezoelectric patches integrated to plate-like harvesters in the literature are limited. De Marqui et al. [43] have studied on an electromechanically coupled finite element model for plate based on Kirchhoff plate assumptions, to obtain power output. In another study, Rupp et al. [44] offered a method for analyzing and designing piezoelectric energy harvesters made up of stacked plates and shells connected to an electrical circuit and they performed topology optimization studies for designing the layout of a multilayer structure. Erturk [45] presented an analytical model for piezoceramic patches utilizing the strain fluctuations of large structures. Aridogan et al. [46] presented analytical electroelastic model of a piezoceramic patch integrated on a thin plate and validated their model by experiments. In another study, the same group have presented coupled electroelastic model for multiple piezoceramic patches integrated on a fully clamped (C-C-C-C) plate and validated their model with experiments [47].

1.3. Review of the Existing Equivalent Circuit Models for Piezoelectric Energy Harvesters Connected to Nonlinear Circuits

In the presence of the non-linear components, the electrical simulation software become very useful to estimate the power output of a such system. At this point, one needs another approach to model the mechanical system in such a way that this mechanical system can be integrated with the non-linear electrical circuit components. Equivalent circuit modelling (ECM) is a modelling type to represent the mechanical part of the harvester in circuit simulator software. In ECM, each vibration mode of the host structure is represented as an individual branch which consists of a resistor, an inductor, and a capacitor which are found by the analogy between mechanical parameters and the second order electrical circuit parameters. In the literature, several methods including analytical and numerical are used to find the ECM parameters. Roundy and Wright [48] have presented a 1-port equivalent circuit model and Cho et al. [49] proposed a 5-port model, but these models do not capture any number of piezoelectric modes. Elvin and Elvin [50] presented analytical approach that can capture any number of piezoelectric modes desired to find equivalent circuit model parameters for beam harvesters. Yang and Tang [51] have proposed a numerical approach to find the equivalent circuit model parameters again for beam harvesters. Bayik et al. [52] have proposed a multi-mode ECM of a piezoelectric patch attached to a thin plate. Aghakhani and Basdogan [53] have extended this model to MPEHs attached on a thin plate. They also integrated their ECM with a rectifier model in SPICE and validated their model both analytically and experimentally. The equivalent circuit model is implemented in a commercial software called LTspice for simulations for this thesis.

1.4. Thesis Outline and Layout

In the literature, the performance improvement achieved by using individual SSHI circuits instead of individual standard rectifier circuits have been studied. However, in the literature, the effect of using different configurations of the SSHI network for multiple piezo patches on plate structures has not yet been understood. This study aims to assess the performance of the networked SSHI configurations compared to networked rectifier configurations and investigate the optimum configurations for energy harvesting purposes. For this research question, four different networked rectifier/SSHI configurations are presented where two of these configurations include a single rectifier/SSHI circuit, and the other two configurations include separate rectifier/SSHI circuits for each patch. The performances of the four configurations are evaluated under harmonic excitation in terms of peak power outputs both experimentally and numerically. For this purpose, the modal analysis is done using the Rayleigh-Ritz method, and the ECM approach is used to simulate the electromechanical system in SPICE software. In chapter 2, the details of the distributed-parameter model of multiple piezo-patches attached on a thin plate and the ECM are given. In chapter 3, the SSHI circuits used in both the experiments and the numerical analyses are discussed. Following, the proposed networked rectifier/SSHI configurations and the experimental setup are presented. Two of these configurations include a single rectifier/SSHI circuit, while the other two configurations include separate rectifier/SSHI circuits for each patch. Later, for the numerical analyses and the integration of rectifier and SSHI circuits, the developed ECM is embedded in LTspice. The proposed configurations are obtained. Chapter 4 presents AC input – AC output and the AC input- DC output results for the simulations and experiments, where thirteen different load resistances are used to narrow down the load resistance steps and find the optimum load resistance for each configuration. The simulation and experimental results are compared to verify the performance trends of different networked rectifier/SSHI configurations. Chapter 5 concludes the thesis with the discussions of the results and future possible studies.

Chapter 2

THE DISTRIBUTED PARAMETER MODEL AND THE EQUIVALENT CIRCUIT MODELING OF MULTIPLE PIEZO-PATCHES ON A THIN-PLATE

2.1. Distributed Parameter Model of Multiple Piezo-patches Attached on A Thin-Plate

In this section, distributed-parameter model is explained briefly for MPEHs attached on a thin-plate based on Kirchhoff plate theory [47]. The model is presented in Figure 2.1. The plate has a length of a, a width of b and a thickness of h_s. As the thickness of the plate is too small compared to its length and width, Kirchhoff plate theory suggests that the transverse shear deformation can be neglected. All four edges of the plate are in clamped (C-C-C-C) position. A transverse point force $f(t)$ is applied at (x_0, y_0) to excite the system. For notation, subscript s is used for plate properties and p is used for piezoceramic properties. The number of piezoceramic patches is $n_{\bar{p}}$, the thickness of the plate is denoted as h_s, the thickness of the piezoceramic harvester is denoted as h_p, and the thickness of kth patch is $\left(h_p\right)_k$. A resistive load is connected to the electrode layers of piezo-patches and denoted as R_l. Since the volume of the PEH is much smaller than the host plate, the contribution of the masses and stiffnesses of the PEHs are neglected, and the patch is integrated as electromechanically.

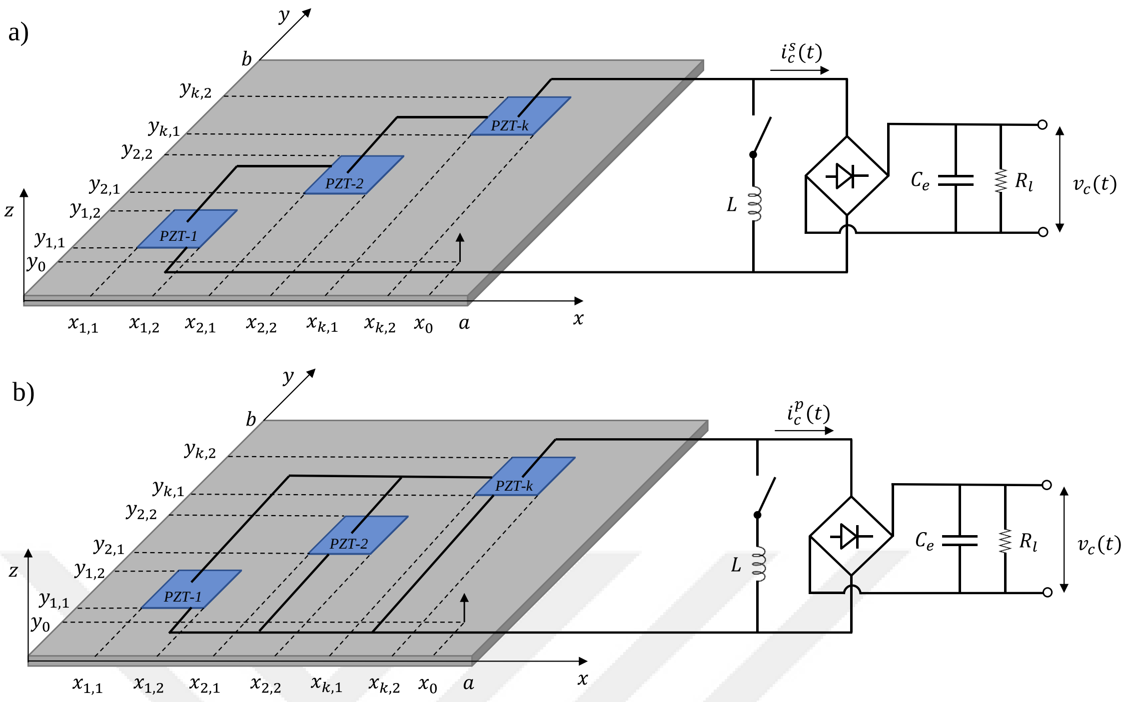

Figure 2.1. Multiple piezo-patch energy harvesters attached on a thin plate integrated with an SSHI circuit: (a) Series configuration (b) Parallel configuration.

The electromechanically coupled equation for a thin plate integrated with MPEHs for transverse force are derived by Aridogan et al. [47].

2.1.1. Electromechanical equations for series configuration

The representation for k piezo-patches which are represented as dependent current sources and connected in series with an SSHI circuit is shown in Figure *2*. Each piezo-patch has an internal capacitance of $\left(C_p\right)_k$. The electrical circuit equation for each PEH can be shown as:

$$(C_p)_k \frac{\mathrm{d}\, v_k^s(t)}{dt} + i_c^s(t) = i_k^s(t) \tag{1}$$

where $k = 1,2,\ldots,n_p$, $v_k^s(t)$ is the voltage across kth piezo-patch, $i_c^s(t)$ is the current passing into the SSHI circuit. The internal capacitance of the kth piezo-patch can be expressed as:

$$(C_p)_k = (\bar{\varepsilon}_{33}^S)_k \frac{(l_p)_k (w_p)_k}{(h_p)_k} \tag{2}$$

where $(\bar{\varepsilon}_{33}^S)_k$ is the permittivity at constant strain, $(l_p)_k$ is the length, $(w_p)_k$ is the width, $(h_p)_k$ is the thickness of the kth piezo-patch.

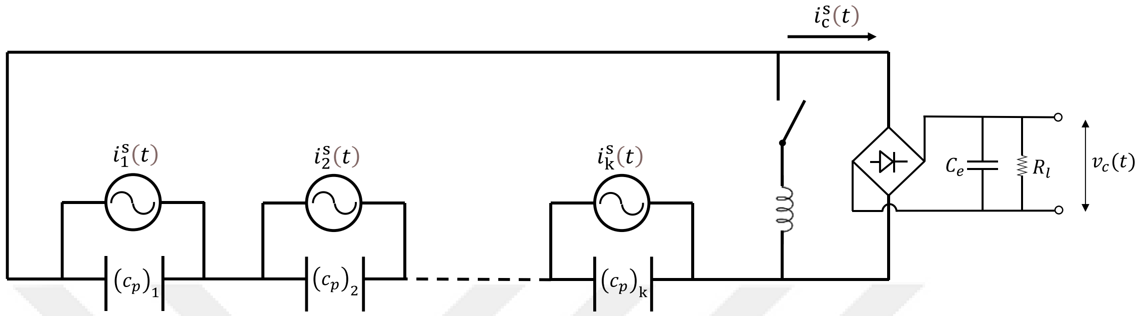

Figure 2.2. Electrical schematic of series connection of MPEHs integrated with an SSHI circuit.

From [47], the electromechanically coupled equations in modal coordinates for series configuration are:

$$\frac{d^2\eta_{mn}^s(t)}{dt^2} + 2\zeta_{mn}\omega_{mn}\frac{d\eta_{mn}^s(t)}{dt} + \omega_{mn}^2\eta_{mn}^s(t) - \sum_{k=1}^{n_p}(\tilde{\theta}_{mn})_k v_k^s(t) = f_{mn}(t) \tag{3}$$

$$\sum_{n=1}^{\infty}\sum_{m=1}^{\infty}(\tilde{\theta}_{mn})_k \frac{d\eta_{mn}^s(t)}{dt} + (C_p)_k \frac{dv_k^s(t)}{dt} + i_c^s(t) = 0 \tag{4}$$

where the mechanical part is represented Eqn. (3) and the electrical part is represented in Eqn. (4). ζ_{mn} and ω_{mn} represents the modal damping ratio and the undamped natural frequency, respectively for the *mn*-th mode. The transverse force in modal coordinates, $f_{mn}(t)$ is [47]:

$$f_{mn}(t) = f(t)\phi_{mn}(x_0, y_0) \tag{5}$$

Using equations (1) and (4), the current source of the kth piezo patch for series configuration can be found as:

$$i_k^s(t) = -\sum_{n=1}^{\infty}\sum_{m=1}^{\infty}(\tilde{\theta}_{mn})_k \frac{d\eta_{mn}^s(t)}{dt} \tag{6}$$

where $\eta^{s}_{mn}(t)$ is the modal coordinate of the plate for the *mn*-th mode and the electromechanical coupling term $(\tilde{\theta}_{mn})_k$ is:

$$(\tilde{\theta}_{mn})_k = \theta_k \int_{y_{k,1}}^{y_{k,2}} \int_{x_{k,1}}^{x_{k,2}} \left[\frac{\partial^2 \phi_{mn}(x,y)}{\partial x^2} + \frac{\partial^2 \phi_{mn}(x,y)}{\partial y^2}\right] dxdy \qquad (7)$$

where $\phi_{mn}(x,y)$ is the mass-normalized eigenfunction of the *mn*-th vibration mode at (x,y) coordinate, electromechanical term for the kth piezo-patch is $\theta_k = (h_{\mathrm{pc}})_k(\bar{e}_{31})_k$. Here, $(\bar{e}_{31})_k$ represents the effective piezoelectric constant and $(h_{\mathrm{pc}})_k$ represents the distance of the center layer of the kth piezo-patch from the reference surface at the location of the kth piezo-patch.

2.1.2. Electromechanical equations for parallel configuration

The representation for k piezo-patches, which are represented as dependent current sources and connected in parallel with an SSHI circuit is shown in Figure 2.3.

$$\frac{\mathrm{d}\, v^{p}(t)}{dt} \sum_{k=1}^{n_{\tilde{p}}} (C_{\tilde{p}})_k + i^{p}_{c}(t) = \sum_{k=1}^{n_{\tilde{p}}} i^{p}_{k}(t) \qquad (8)$$

In Equation (8), $v^{p}(t)$, $i^{p}_{c}(t)$ represents the voltage across each piezo-patch electrodes and the current passing through the SSHI circuit, respectively. The equivalent piezoelectric capacitance, which is denoted as $(C_{\tilde{p}})_k$ is same as (2). The current source equation can be written as:

$$i^{p}_{k}(t) = -\sum_{n=1}^{\infty} \sum_{m=1}^{\infty} (\tilde{\theta}_{mn})_k \frac{d\eta^{p}_{mn}(t)}{dt} \qquad (9)$$

where, $\eta^{p}_{mn}(t)$ is the modal coordinate for the *mn*-th mode and the electromechanical coupling term $(\tilde{\theta}_{mn})_k$ is same as (7).

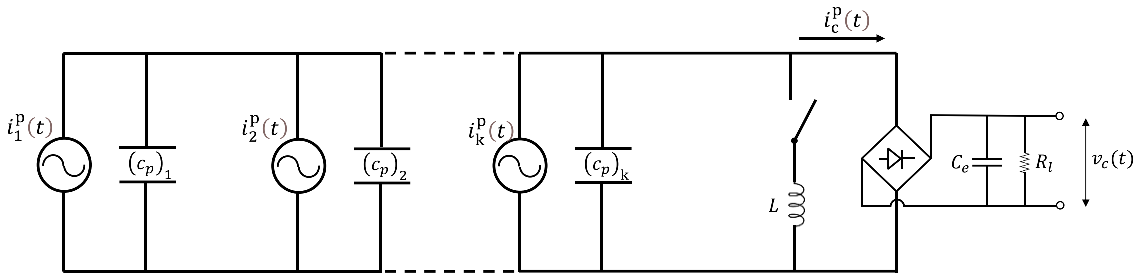

Figure 2.3. Electrical schematic of parallel connection of MPEHs integrated with an SSHI circuit.

From [47], the electromechanically coupled equations in modal coordinates for parallel configuration can be expressed as

$$\frac{d^2\eta_{mn}^p(t)}{dt^2} + 2\zeta_{mn}\omega_{mn}\frac{d\eta_{mn}^p(t)}{dt} + \omega_{mn}^2\eta_{mn}^p(t) - \sum_{k=1}^{n_p}(\tilde{\theta}_{mn})_k v_k^s(t) = f_{mn}(t) \tag{10}$$

$$\sum_{k=1}^{n_{\bar{p}}}\sum_{n=1}^{\infty}\sum_{m=1}^{\infty}(\tilde{\theta}_{mn})_k\frac{d\eta_{mn}^p(t)}{dt} + \frac{dv^p(t)}{dt}\sum_{k=1}^{n_{\bar{p}}}(C_{\bar{p}})_k + i_c^p(t) = 0 \tag{11}$$

The transverse force in modal coordinates which is represented as $f_{mn}(t)$ is same as (5).

2.2. Equivalent Circuit Modeling Overview

Piezo-patch energy harvesters linked to thin plates may be easily incorporated to plate-like structures in automotive, marine, and aerospace applications in order to directly utilize structural vibrations of the host system. In the earlier studies, researchers used a resistive load to find the AC power output [43, 46, 47, 54]. However, the situation is different when it comes to practical purposes like transferring the power to a storage capacitor. For practical purposes, the alternating current obtained from energy harvesting should be transformed to a more stable form. For this purpose, with the help of a rectifier bridge and a smoothing capacitor, the alternating current (AC) is transformed to a steady rectified direct current (DC). For most of these transformations, a full wave AC-DC rectifier is used. In addition to this AC-DC transformation, it is advantageous to use a smoothing capacitor to improve the performance where the smoothing capacitor acts as a DC-DC converter [55].

In the presence of the non-linear components, the electrical simulation software (such as SPICE) becomes very handy to estimate the power output of such system. For using these software, the mechanical system should be modeled in such a way that it can be integrated with the non-linear electrical circuit components. Equivalent circuit modelling (ECM) is a modeling type to represent the mechanical part of the harvester in circuit simulator software SPICE. In ECM, each vibration mode of the host structure is represented as an individual branch which consists of a resistor, an inductor, and a capacitor which are found by the analogy between mechanical parameters and the second order electrical circuit parameters. For plate-like structures, Bayik et al. [52] have proposed a multi-mode ECM of a piezoelectric patch attached to a thin plate and found the equivalent circuit parameters both by analytical and numerical approaches. Aghakhani and Basdogan [53] have extended this model to MPEHs attached on a thin-plate. In the following section, the equivalent circuit modeling (ECM) of multiple piezo-patches attached on a thin-plate will be explained.

2.3. Equivalent Circuit Analogy

The analogy between mechanical domain and electrical domain connections serves as the foundation for the equivalent circuit analogy of piezoelectric energy harvesters. A mechanical and electrical system analogous to each other are presented in Figure 2.4.

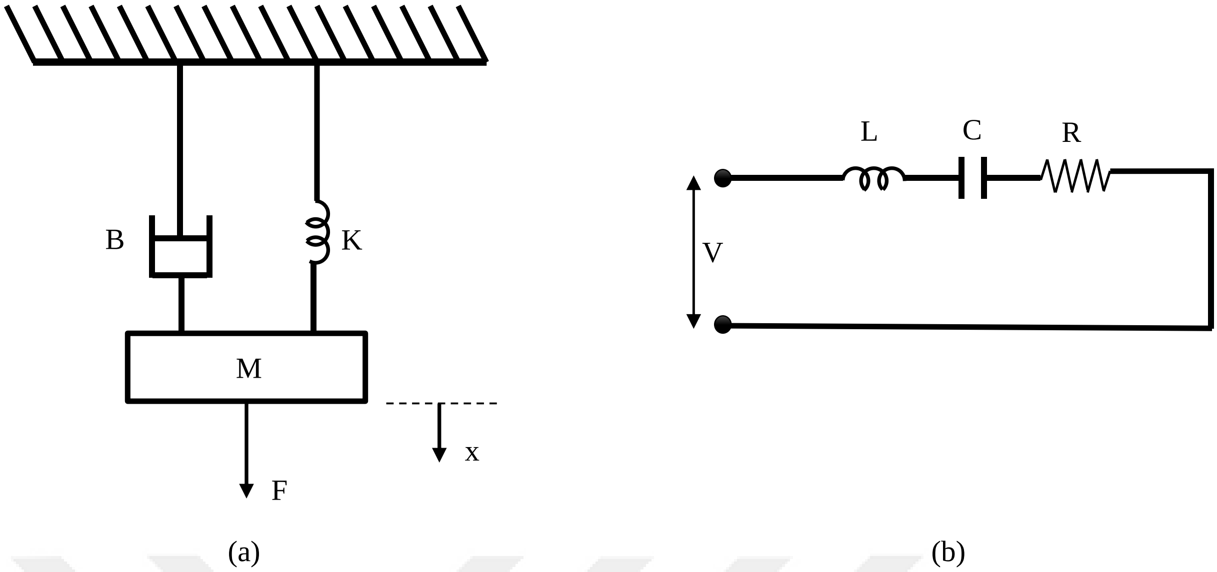

Figure 2.4. Mechanical (a) and electrical (b) representation of a system.

The force balanced equation for the mechanical system is:

$$F = M\frac{d^2x}{dt^2} + B\frac{dx}{dt} + Kx \tag{1}$$

and the mesh equation for the electrical system is:

$$V = Ri + L\frac{di}{dt} + \frac{1}{C}\int i\,dt \tag{2}$$

where

$$i = \frac{dq}{dt} \tag{3}$$

After substituting Equation 3 into Equation 2, we get:

$$V = R\frac{dq}{dt} + L\frac{d^2q}{dt^2} + \frac{q}{C} \tag{4}$$

Using the force-voltage analogy, the analogy between the mechanical and the electrical system is presented in Table 2.1.

Table 2.1. Analogy of mechanical and electrical systems.

Mechanical System	Electrical System
Force	Voltage
Displacement	Charge
Velocity	Current
Mass	Inductance
Frictional Coefficient	Resistance
Stiffness	1/Capacitance

2.4. Equivalent Circuit Model of Multiple Piezo-patches Attached on a Thin-plate

Equivalent circuit modeling is a technique where each mode of the structure is represented with a second-order circuit. This second-order circuit consists of a resistor, an inductor, and a capacitor which are found by the analogy between mechanical parameters and the second order electrical circuit parameters. In Figure 2.5, the equivalent circuit model of the plate coupled with a piezo-patch is presented. Here, each branch consisting of a voltage source, an inductor, a capacitor, and a resistor represents a vibration mode, where there are $m \times n$ modes in total. Each set of secondary-order circuits can also be represented dependent current sources in the literature [53] which contain voltage, inductor, capacitor and the resistor of their respective modes in them. As every schematic represents a single PEH, this schematic needs to be repeated for the MPEH case.

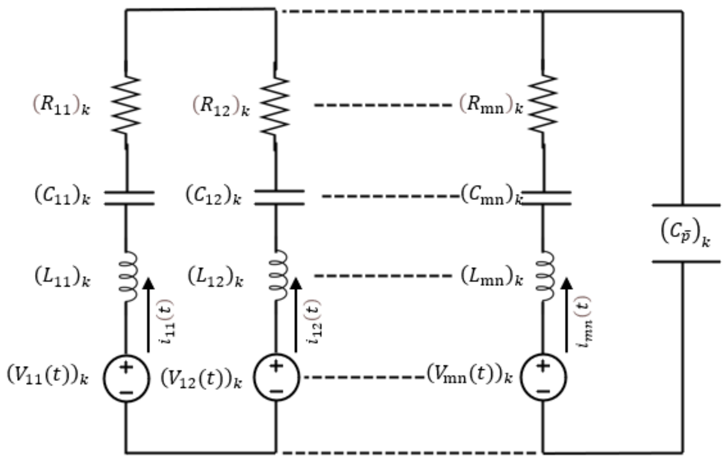

Figure 2.5. Equivalent circuit model of the plate coupled with a piezo-patch, where each branch represents a mode (m×n modes in total).

The second-order equivalent circuit model parameters and the mechanical counterparts for MPEHs can be found as shown in Table 2.2 [53] after applying Kirchhoff's voltage law and analogy with the electromechanically coupled equations in modal coordinates for series and parallel configurations [47].

Table 2.2. Equivalent Circuit Modeling Parameters and Their Mechanical Counterparts.

Equivalent circuit parameters for the *mn*-th vibration mode of *k*-th piezo-patch harvester	Mechanical counterparts
Voltage source: $(v_{mn}(t))_k$	$-\dfrac{f_{mn}(t)}{\sum_{k=1}^{n_{\bar{p}}}(\tilde{\theta}_{mn})_k}$
Electrical current: $(i_{mn}(t))_k$	$-(\tilde{\theta}_{mn})_k\dot{\eta}_{mn}^{p}(t)$ (parallel) $-(\tilde{\theta}_{mn})_k\dot{\eta}_{mn}^{s}(t)$ (series)
Inductance: $(L_{mn})_k$	$\dfrac{1}{(\tilde{\theta}_{mn})_k\sum_{k=1}^{n_{\bar{p}}}(\tilde{\theta}_{mn})_k}$
Resistance: $(R_{mn})_k$	$\dfrac{2\zeta_{mn}\omega_{mn}}{(\tilde{\theta}_{mn})_k\sum_{k=1}^{n_{\bar{p}}}(\tilde{\theta}_{mn})_k}$
Capacitance: $(C_{mn})_k$	$\dfrac{(\tilde{\theta}_{mn})_k\sum_{k=1}^{n_{\bar{p}}}(\tilde{\theta}_{mn})_k}{\omega_{mn}{}^2}$

Chapter 3

THE NETWORKED CONFIGURATIONS AND THE EXPERIMENTAL SETUP

3.1. SSHI Circuit Schematic and The Networked Configurations

In this section, four different networks for three piezoelectric energy harvesters are presented. These configurations are explained in the proceeding sections. The schematic of the SSHI circuit used in the simulations is presented in Figure 3.1, which is a type of parallel-SSHI (p-SSHI). Diodes used in this circuit are characterized as they have a forward voltage drop as 0.25 V, to represent the BAT46W fast recovery Schottky diodes. The circuit elements in the SSHI circuit is tabulated in Table 3.1 and the switching device of the SSHI circuit embedded in LTspice is shown in Figure 3.2.

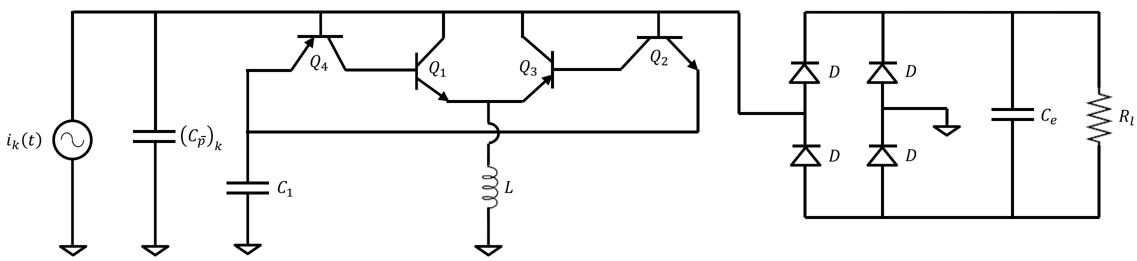

Figure 3.1. SSHI Circuit Schematic.

Table 3.1. SSHI Circuit Elements.

SSHI Circuit Elements	Their Values / Models
C_1	1 nF
L	100 mH
Q_1 & Q_2	2SC2412K NPN Transistor
Q_3 & Q_4	2SA2029 PNP Transistor
C_e	5 µF

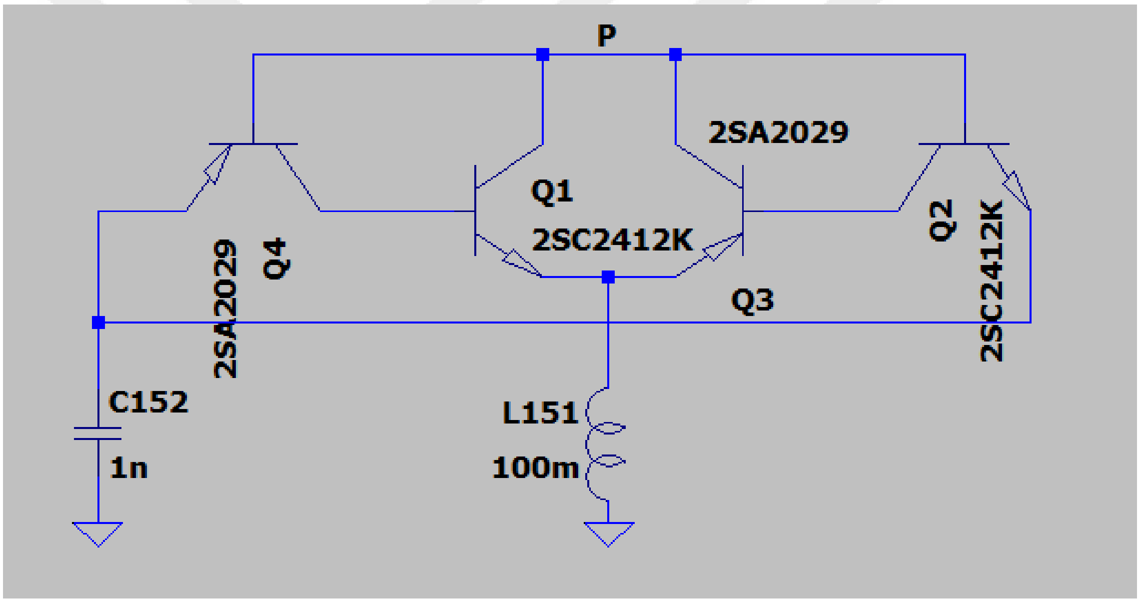

Figure 3.2. SSHI circuit switching device in LTspice.

The networked configurations are presented Figure 3.3. The rectifier and SSHI circuits are denoted as $Z_{circuit}$ for simplicity.

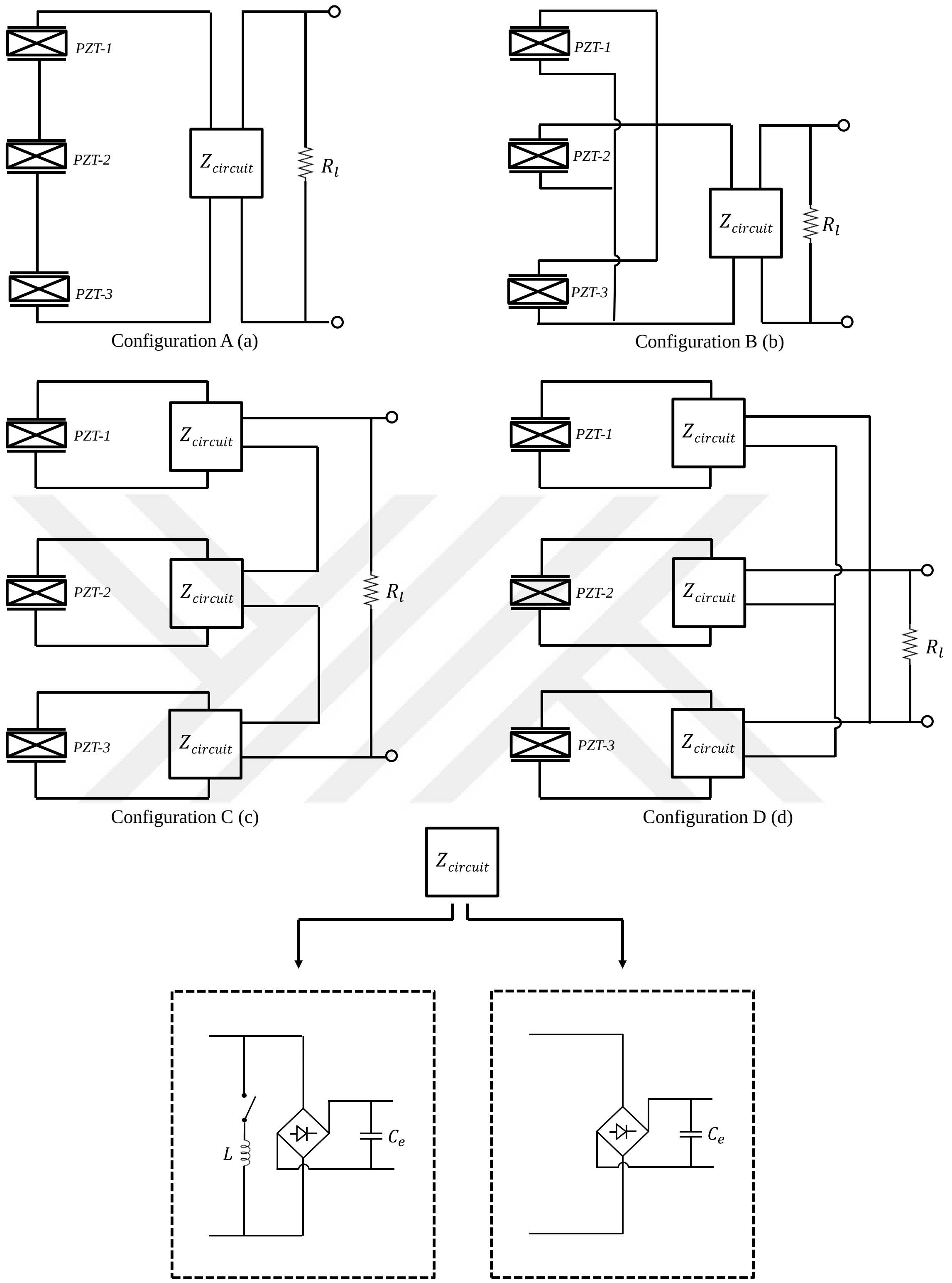

Expansion of $Z_{circuit}$ as SSHI and rectifier circuits (e)

Figure 3.3. The circuit models for all configurations and the expansion of $Z_{circuit}$. (a) Configuration A: Multiple series patches – single rectifier/SSHI. (b) configuration B: Multiple parallel patches – single SSHI. (c) Configuration C: Multiple patches – multiple

series rectifiers/SSHIs. (d) Configuration D: Multiple patches – multiple parallel rectifiers/SSHIs. (e) SSHI and rectifier circuit components.

In configuration A, presented in Figure 3.3(a), three piezo-patches are connected in series and a single rectifier/SSHI circuit is integrated into the series configuration of the piezo-patches. This configuration will be a reference for comparison with configurations where multiple rectifiers/SSHIs are used in the upcoming sections.

Figure 3.3(b) presents configuration B, where three piezo-patches are connected in parallel, and a single rectifier/SSHI circuit is integrated into the parallel configuration of the piezo-patches. As there is only a single rectifier/SSHI circuit, all three piezo-patches are contributing to a single waveform in this configuration, just like configuration A. Therefore, the waveform of this more complex.

In Figure 3.3(c), configuration C is presented where each piezo-patch has been integrated with a rectifier/SSHI circuit, and the output of those rectifier/SSHI circuits are connected in series. There are separate capacitors for each piezo-patch and the output voltage $V_c(t)$ is the sum of the outputs of three SSHI circuits. Due to this summation, this configuration is expected to result in higher voltage outputs for higher load resistances.

Configuration D, which consists of multiple rectifier/SSHI circuits connected in parallel is presented in Figure 3.3(d). Similar to configuration C, there are separate capacitors for each piezo-patch, and the output voltage on R_l is expected to be determined by the most dominant piezo-patch for that particular frequency.

3.2. The Experimental Setup

The experimental setup to verify the energy harvesting performance of the configurations is presented in Figure 3.4. A rectangular aluminum plate is used as the host plate, and all four edges are clamped by tightening the screws on the clamping frame. Three transversely isotropic piezoceramic patches (T105-A4E-602 manufactured by Piezo Systems, Inc.) are bonded as piezo-patch energy harvesters on the host plate. The aluminum plate is excited by a modal shaker at 0.085 m to the left and 0.085 m to the up from the right bottom corner, and the dynamic point force acting on the plate is measured by a force transducer (PCB 208C02). The transverse velocity outputs are measured by a laser Doppler vibrometer (Polytec PDV 100). At the first stage of the experiment, AC input - AC output analyses were performed by applying a linear sine sweep for 40-195 Hz range for open-circuit ($R_l = 1M\Omega$) condition. For the second stage, the configuration performances have been analyzed by applying sine sweep at the narrow bandwidths for each mode one-by-one, where the bandwidths are selected as the power outputs are above a considerable level. The sweep rate has been chosen to be slow enough to allow the smoothing capacitor charge and fast enough to prevent unnecessarily big experimental data to be saved.

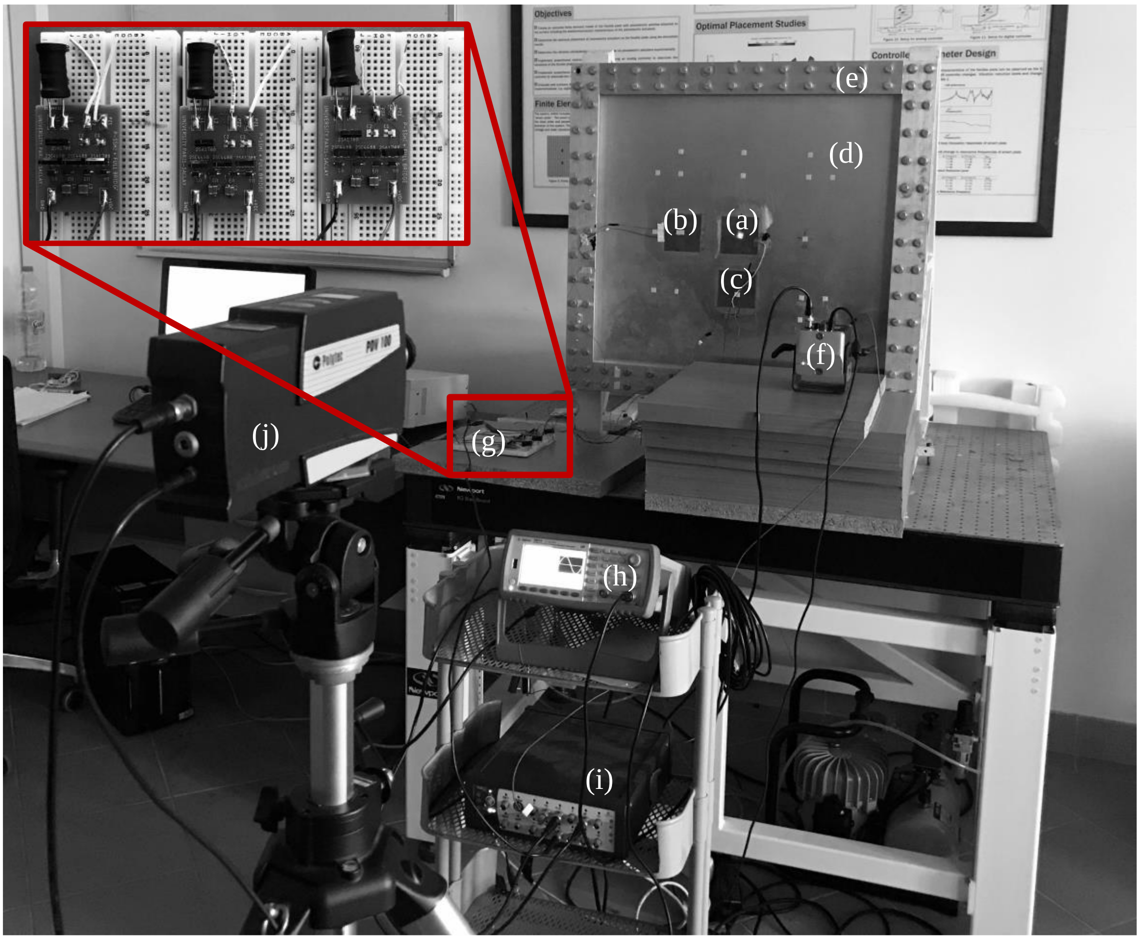

Figure 3.4. Experimental setup: (a) PZT-1, (b) PZT-2, (c) PZT-3, (d) aluminum host plate, (e) clamping frames, (f) shaker with a force transducer, (g) SSHI circuits, (h) signal generator, (i) data acquisition unit and (j) laser vibrometer.

The geometric and material properties of the host plate and the piezoceramics are presented in Table 3.2.

Table 3.2. Geometric and material properties of the host plate and the piezoceramics.

Properties	Aluminum Plate	Piezoceramic
Length (mm)	580	72.4
Width (mm)	540	72.4
Thickness (mm)	1.9	0.267
Young's Modulus (GPa)	65.1	66
Mass Density (kg m^{-3})	2575	7800
Piezoelectric Constant d^{31} (pm V^{-1})	-	-190
Permittivity Constant $\bar{\varepsilon}_{33}^{s}$ (Nf m^{-1})	-	10.38

3.3. Mode Shapes of The Structure

The dynamic strain distribution plays an important role in energy harvesting of by piezoelectric materials. In the case of utilization of multiple piezoelectric energy harvesters, to power output of the harvesters might be very low due to the charge cancellation occurrence if the signs of strain distribution under the patches are opposite. To better understand the effect of charge cancellation, the mode shapes of the structure need to be considered. The mode shapes of the three piezo-patches attached on a thin-plate structure is presented in Figure 3.5, where the three piezo-patches are shown as gray shaded areas. As can be observed, the signs of the strain distributions are same for the first mode. This results in no charge cancellation for this mode. For the second and third mode, the charge cancellation is relatively higher compared to the first mode. And for the fourth mode and fifth mode, the charge cancellation is expected to be more dominant due to the complex dynamics of the mode shapes.

As charge cancellation is expected to be a prominent problem in cases where only a single harvester circuit is used, the utilization of respective circuits is expected to result in higher power outputs.

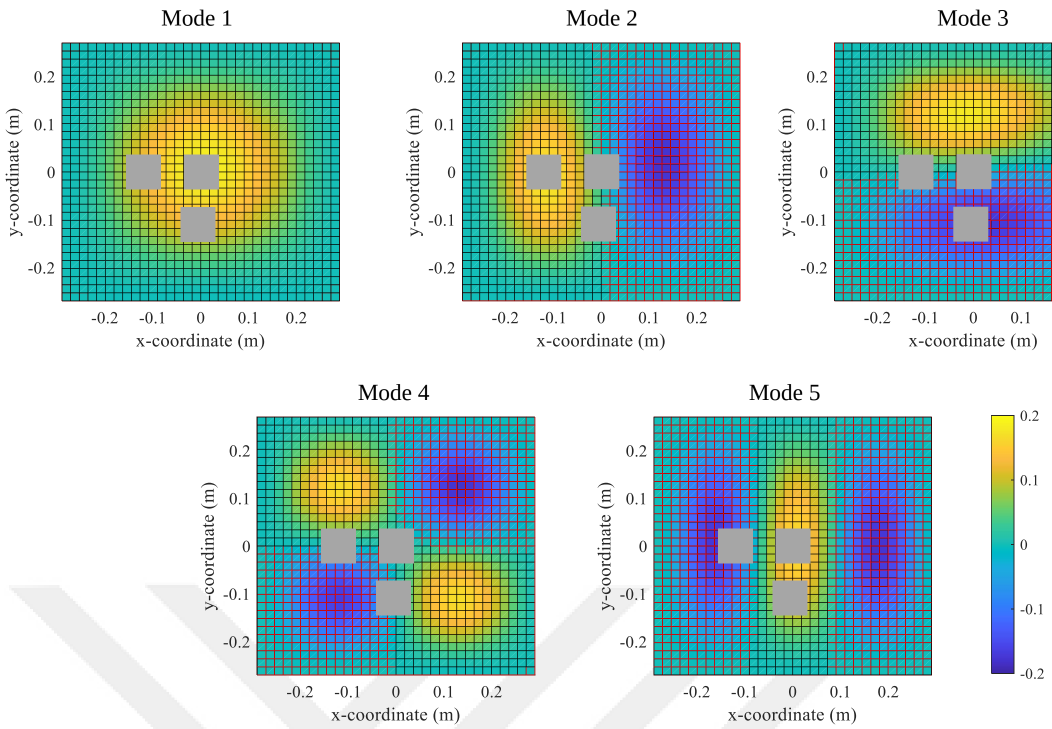

Figure 3.5. Normalized strain mode shapes of the structure for the first five modes.

Chapter 4

EQUIVALENT CIRCUIT MODEL VERIFICATION AND THE HARVESTING PERFORMANCE ANALYSES OF THE NETWORKED CONFIGURATIONS

4.1. AC input – AC output verifications

Parameters of the signal generator for the AC input-AC output experiments have been shown in Figure 4.1, and the results have been compared and presented in Figure 4.2 for open-circuit ($R_l = 1M\Omega$) condition both for experimental and numerical analyses from 40 Hz to 195 Hz.

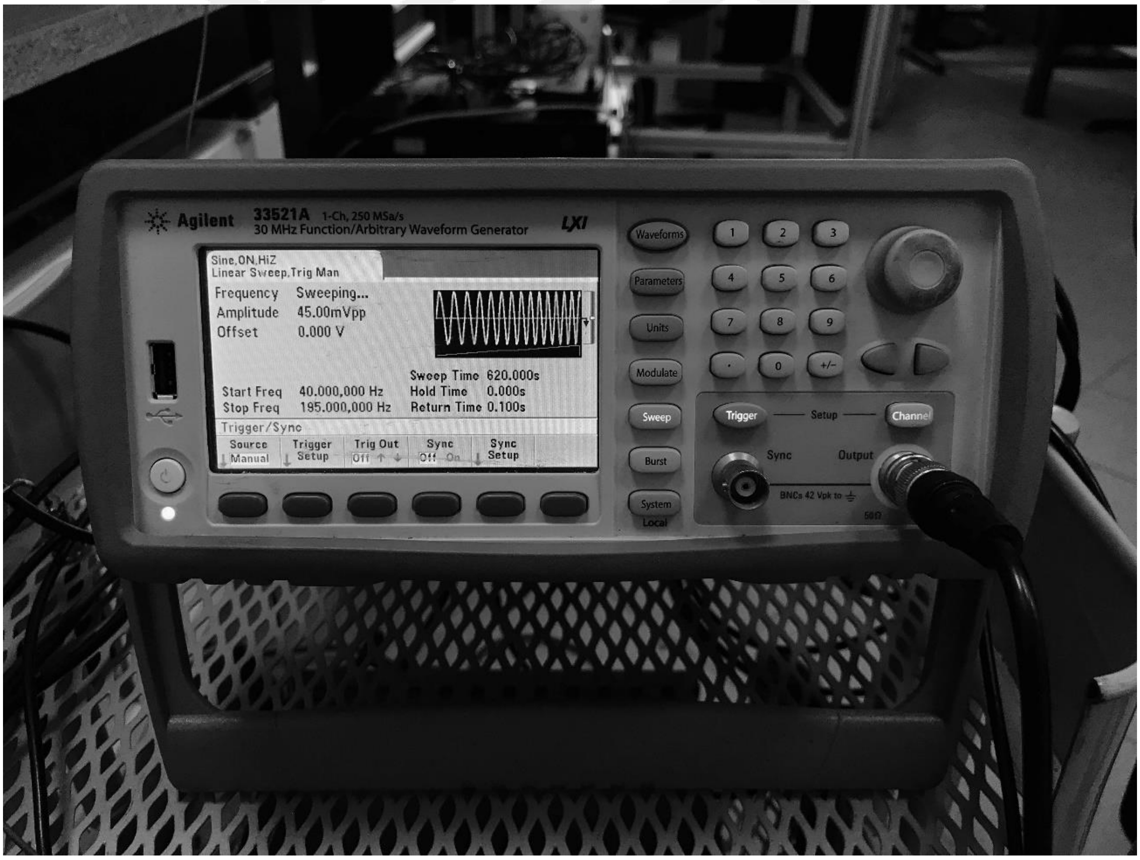

Figure 4.1. Parameters of the signal generator for the AC input-AC output experiments.

The modal damping ratios are extracted from the experimental voltage FRFs, and an equivalent circuit model considering the first 20 modes of the plate is used for the numerical analyses which are performed in the electrical circuit simulation software LTspice. As it can be observed, the LTspice simulations match the experimental analyses in terms of the natural frequencies and the voltage outputs firmly, except the trivial frequency shift in the third mode. The discrepancies between the numerical and experimental models can be explained by the difficulty of achieving a perfect clamping and the experimental room conditions, which affect the modal parameters. Also, the aluminum plate parameters are taken from material tables, and these can be slightly different than the plate used in the experiments.

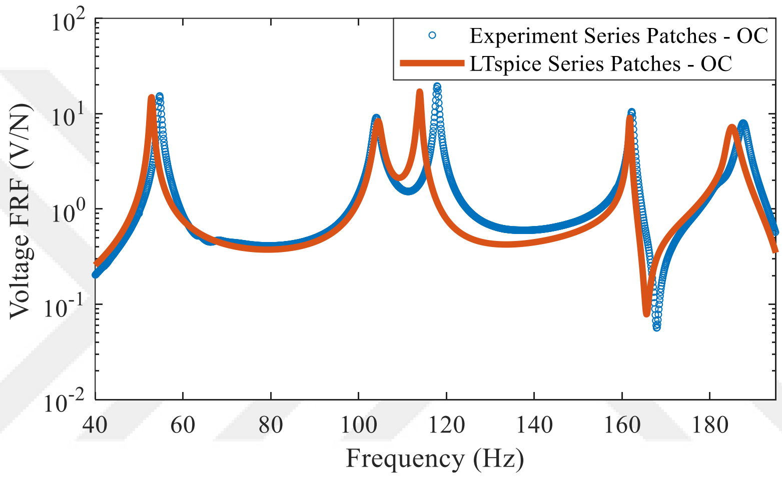

(a)

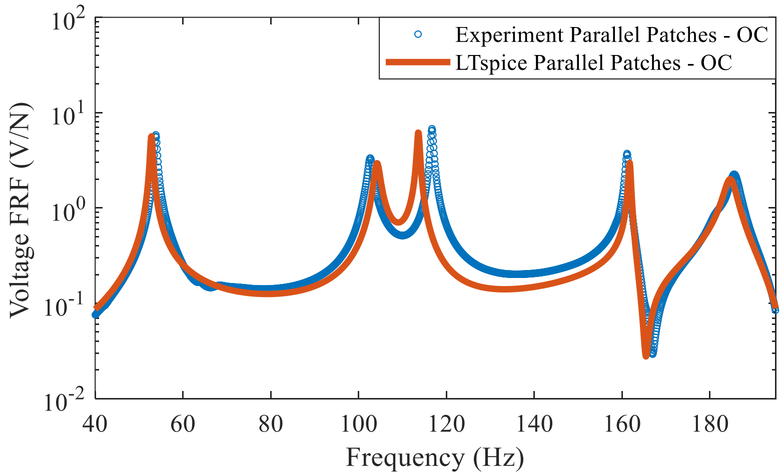

(b)

Figure 4.2. Comparison of experimental and numerical model for the AC input- AC output case. Three piezo-patches are connected in series (a) and parallel (b) configurations, and a load resistance of 1MΩ is connected to the output of the configurations.

4.2. AC input – DC output verifications

In this section, the simulation and experimental results for three piezo-patches attached to a thin plate and integrated with the aforementioned networked rectifier/SSHI configurations are shared where the generated ECM and the SSHI configurations are integrated in LTspice. For the AC input – DC output numerical analyses, the standard rectifier circuit and the SSHI circuit in Figure 3.1 is used for all configurations. Voltage frequency response functions (FRFs) are presented in Figure 4.3 for the four different networked SSHI configurations, where the thirteen different resistive loads ranging from 1 kΩ to 1 MΩ are used for the analyses. The plate is excited with a harmonic force with an amplitude of 1 N, and the output voltages are measured. The LTspice model of the SSHI circuit has been integrated with the ECM of the plate, where the circuit elements are chosen similar to the experimental SSHI circuit. Despite some assumptions made in the diode and SSHI circuit modeling, the results obtained from LTspice simulations closely match the experimental results. It can be observed that the natural frequency of the plate structure has been shifted by an amount in configuration C and D. This is due to the experimental room conditions where the changes in the temperature of the room change the natural frequency of the structure [56].

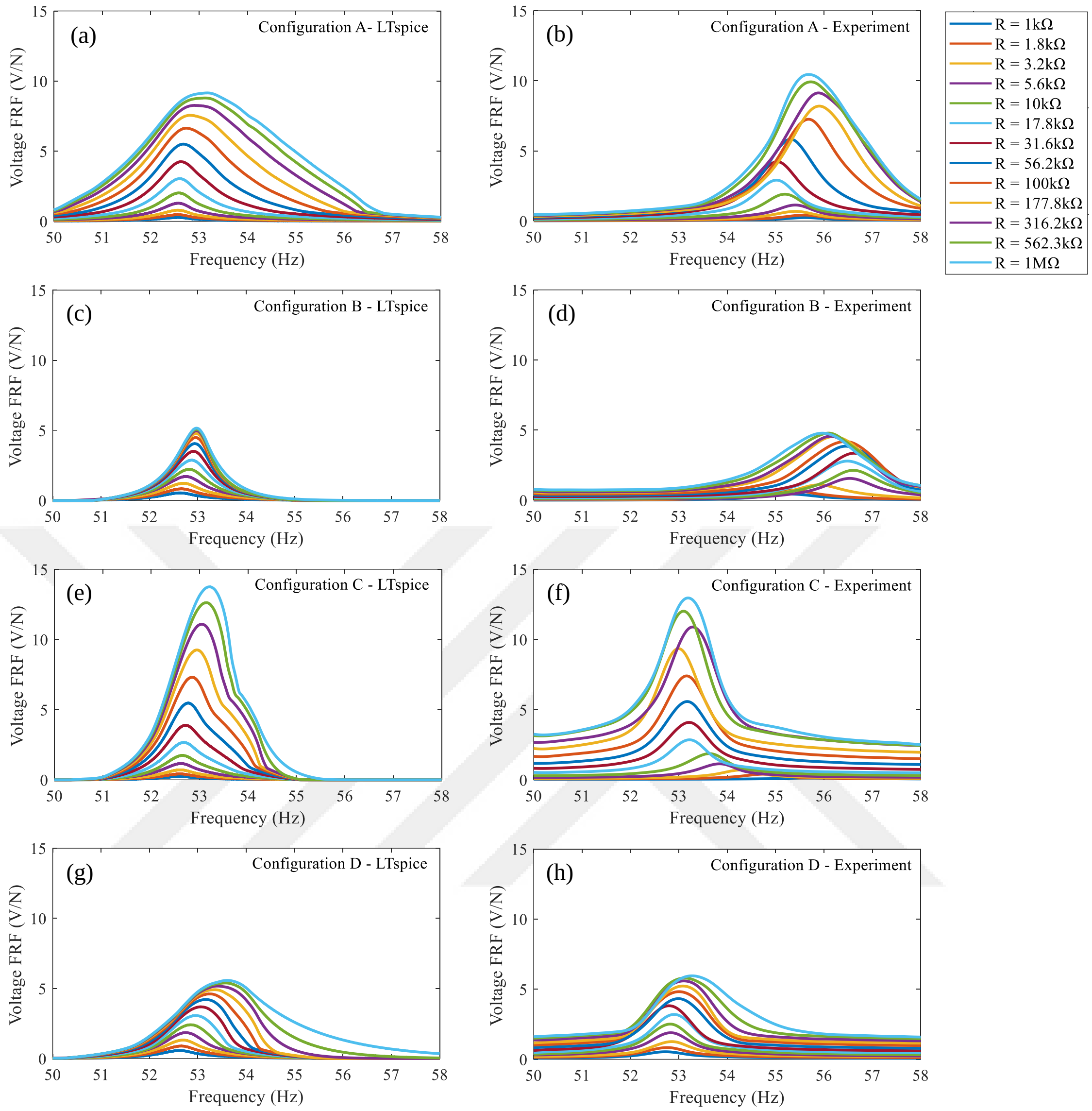

Figure 4.3. LTspice and experiment results presenting the variations of voltage FRFs (V/N) of the four different configurations for networked SSHI; configuration A: LTspice (a) and experiment (b); configuration B: LTspice (c) and experiment (d); configuration C: LTspice (e) and experiment (f) and configuration D: LTspice (g) and experiment (h) for thirteen load resistances ranging from 1kΩ to 1MΩ.

Considering the AC input – AC output results in Figure 4.2 and AC input – DC output results in Figure 4.3, it can be said that the numerical model captures the modes and the trend of voltage outputs for the first five modes and therefore can be used as a useful tool to evaluate the power output for the possible future case studies as well.

To assess the performance of the networked SSHI configurations, one can use the performance of the networked rectifier configurations as a reference. Since the utilization of multiple rectifiers/SSHI circuits and different load resistances induce a slight variation in resonance frequency, instead of directly calculating the power value at a specific frequency, frequency sweeps have been performed for narrowed frequency ranges for each mode, and the peak power values are recorded. These peak powers of the four different networked rectifier and networked SSHI configurations versus varying thirteen resistances from 1kΩ to 1MΩ have been presented in Figure 4.4.

All three piezo-patches have the same internal capacitance, which is 247 nF. As stated by Erturk and Inman [3], the equivalent piezoelectric capacitance and the optimum load resistance have an inverse proportion. This is the reason why configuration A and C responds with higher peak powers in higher load resistances compared to configuration B and D, which respond better in lower load resistances. This phenomenon can be useful to match the impedance of the sensor device to be powered.

The improvement of the peak power outputs after using networked SSHI instead of networked rectifier is tabulated in Table 4.1. The results indicate that the networked SSHI configurations outperform networked rectifier configurations when the average power improvements are accounted in experiments for each configuration. In order to compare the performances of the different networked SSHI configurations, the experimental peak power outputs of each configuration for the first five modes are presented in Table 4.2. The optimal configuration is determined by comparing the peak power levels of each configuration and expressing their power improvement percentage with configuration A as the reference. As it can be observed, the peak power values are far smaller for single SSHI configurations compared to multiple SSHI configurations in some of the modes. The reason of this is the charge cancelation since the collected charge output on the electrode layers of the piezo-patches is determined by the strain distribution, and with the current positions of the piezo-patches, the charges might cancel each other for these modes [47]. In the cases where multiple piezo-patches are connected, the voltage phases should be considered if a single SSHI is to be used. The imaginary part of the voltage FRF of each patch should match in terms of their signs to maximize the voltage output, thus power output. For the modes where there is negligible charge cancelation, e.g., first mode, the benefit of multiple SSHI circuits disappears. In addition, due to the voltage drop from the non-linear diodes in the SSHI circuits, the harvesting performance is affected negatively in terms of power outputs, as the voltage drop will be approximately three times higher than the single SSHI circuit cases. As charge cancelation occurs especially in the higher modes due to the opposite signs of strain distribution under the piezoelectric patches, configuration C and D result in higher power outputs.

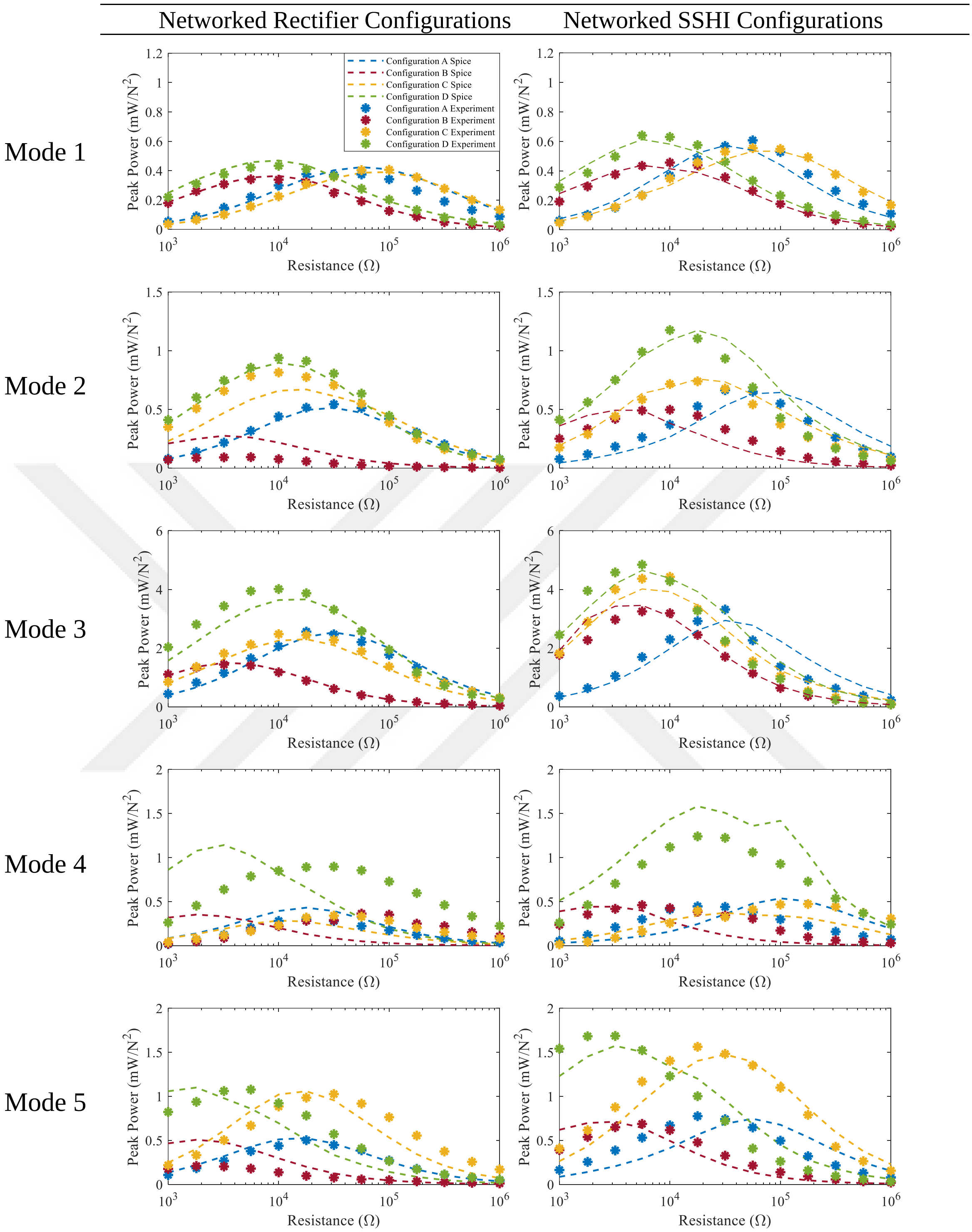

Figure 4.4. Comparison of peak power outputs of the four configurations of networked rectifier and networked SSHI versus varying resistances from 1 kΩ to 1 MΩ for the first five modes; both experimental and numerical results.

Table 4.1. Improvement/deterioration of the experimental peak power outputs after using networked SSHI circuit instead of networked rectifier circuit.

Modes and Average Improvement	Configuration A Peak Power Improvement (%)	Configuration B Peak Power Improvement (%)	Configuration C Peak Power Improvement (%)	Configuration D Peak Power Improvement (%)
Mode 1	61	34	37	48
Mode 2	22	428	-9	25
Mode 3	29	126	78	21
Mode 4	46	26	37	38
Mode 5	55	223	52	56
Average Improvement	42.6	167.4	39.0	37.6

Table 4.2. Experimental peak power outputs of the four networked SSHI configurations.

Modes	Configuration A Peak Power (mW/N^2)	Configuration B Peak Power (mW/N^2)	Configuration C Peak Power (mW/N^2)	Configuration D Peak Power (mW/N^2)	The Best Config. & Improvement (Config. A as ref.)
Mode 1	0.61	0.45	0.55	0.64	D (4.9%)
Mode 2	0.66	0.50	0.74	1.18	D (78.8%)
Mode 3	3.32	3.25	4.43	4.84	D (45.8%)
Mode 4	0.44	0.46	0.47	1.24	D (181.8%)
Mode 5	0.78	0.68	1.56	1.68	D (115.4%)

Chapter 5

SUMMARY, CONCLUSION AND FUTURE WORK

Over the last decades, there has been an intense interest in vibration-based energy harvesting as a means of producing electricity for use in small electrical devices and components. In years, patch-based piezoelectric energy harvesters became popular as the multimodal vibrations in aerospace, automotive and marine applications can be extracted by piezo-patches. For the AC-DC transformation of the harvested energy, researchers have focused on different circuit designs including synchronized switch harvesting on inductor (SSHI) to improve the output power compared to standard rectifier circuits. In the literature, it was shown that the SSHI circuit can boost the harvested power when used instead of standard rectifier circuits for each piezo-patch. However, yet to this study, it was unclear how employing various SSHI network configurations for several piezo-patches may affect the harvesting performance. The purpose of this thesis is to determine the best configurations for energy harvesting and to evaluate the performance of networked SSHI configurations to networked rectifier configurations.

In Chapter 1, piezoelectric energy harvesting was introduced and the previous studies in the literature were reviewed.

In Chapter 2, the distributed-parameter model, which is the basis of the equivalent circuit model (ECM) is explained. By applying analogy between the electromechanical equations and second-order electrical circuits, equivalent circuit model of the electromechanical system is developed.

In Chapter 3, SSHI circuits used in the simulations are presented. Later, four different networked rectifier and networked SSHI configurations were presented, where two of these configurations include a single rectifier/SSHI circuit, and the other two configurations include separate rectifier/SSHI circuits for each patch. The experimental setup is shown where three piezo-patches are bonded with the thin aluminum host plate. Subsequently, to integrate the electromechanical system with non-linear circuits, the developed equivalent circuit model is embedded in LTspice software, and the proposed configurations are developed in LTspice with the integration of rectifier/SSHI circuits.

In Chapter 4, the performances of each configuration are evaluated under harmonic excitation in terms of peak power outputs, and the optimal load resistances are identified. The experimental results are compared in relation to the peak power changes observed when SSHI circuits are employed instead of rectifier circuits in networked configurations. The results are presented, which demonstrates that the SSHI circuits significantly improve the output power when compared to the rectifier circuits in the networked configurations. The most severe improvement is observed in configuration B, by 167.4%. Subsequently, the results are compared in terms of the peak power outputs of the four different networked SSHI configurations. The results show that when configuration D instead of configuration A which is the reference configuration, the power output has increased by 4.9%, 78.8%, 45.8%, 181.8%, and 115.4% for the first, second, third, fourth, and fifth modes, respectively. The findings demonstrate that by using respective SSHI circuits, the power output is significantly boosted for the modes charge cancellation occurs. Furthermore, for these modes, depending on the impedance of the sensor device, the selection can be made between configuration C and configuration D by accounting for the power output differential between the two configurations.

As future work, the proposed networked configurations can be demonstrated in real life applications. The advantage of using such networked configurations is highly possible to be prominent in large structures. As enlarging the size of the piezoceramics is not something feasible in certain operations, the real-life application of such networked configurations can be beneficial. In addition, a practical application of the proposed configurations might be reasonable under broadband excitations. Furthermore, a switching mechanism can be designed and added to the configurations for the modes that there is no charge cancellation and the diode loss caused by respective circuits can be reduced by dropping the harvesting circuit number. Another future work can be stated as the miniaturization of SSHI circuits to use them on wearable applications. Since using respective circuits might not be practicable for small scale applications, the size of the SSHI circuits can be a problem and needs to be scaled down. Moreover, an analytical model can be developed for networked SSHI configurations, and the power output can be estimated.

BIBLIOGRAPHY

[1] J. Chen and Z. L. Wang, "Reviving vibration energy harvesting and self-powered sensing by a triboelectric nanogenerator," *Joule,* vol. 1, no. 3, pp. 480-521, 2017.

[2] J. A. Paradiso and T. Starner, "Energy scavenging for mobile and wireless electronics," *IEEE Pervasive computing,* vol. 4, no. 1, pp. 18-27, 2005.

[3] A. Erturk and D. J. Inman, *Piezoelectric energy harvesting*. John Wiley & Sons, 2011.

[4] E. O. Torres and G. A. Rincón-Mora, "Electrostatic energy-harvesting and battery-charging CMOS system prototype," *IEEE Transactions on Circuits and Systems I: Regular Papers,* vol. 56, no. 9, pp. 1938-1948, 2008.

[5] C. Lee *et al.*, "Theoretical comparison of the energy harvesting capability among various electrostatic mechanisms from structure aspect," *Sensors and Actuators A: Physical,* vol. 156, no. 1, pp. 208-216, 2009.

[6] C. A. Howells, "Piezoelectric energy harvesting," *Energy Conversion and Management,* vol. 50, no. 7, pp. 1847-1850, 2009.

[7] C. Graf, J. Maas, and D. Schapeler, "Energy harvesting cycles based on electro active polymers," in *Electroactive Polymer Actuators and Devices (EAPAD) 2010*, 2010, vol. 7642: SPIE, pp. 362-373.

[8] L. Wang and F. Yuan, "Vibration energy harvesting by magnetostrictive material," *Smart Materials and Structures,* vol. 17, no. 4, p. 045009, 2008.

[9] F. Narita and M. Fox, "A review on piezoelectric, magnetostrictive, and magnetoelectric materials and device technologies for energy harvesting applications," *Advanced Engineering Materials*, vol. 20, no. 5, p. 1700743, 2018.

[10] E. Maghsoudi Nia, N. Wan Abdullah Zawawi, and B. Mahinder Singh, "Design of a pavement using piezoelectric materials," *Materialwissenschaft und Werkstofftechnik,* vol. 50, no. 3, pp. 320-328, 2019.

[11] P. Dineva *et al.*, *Piezoelectric materials*. Springer, 2014.

[12] H. A. Sodano, D. J. Inman, and G. Park, "Comparison of piezoelectric energy harvesting devices for recharging batteries," *Journal of intelligent material systems and structures,* vol. 16, no. 10, pp. 799-807, 2005.

[13] T. J. Johnson, D. Charnegie, W. W. Clark, M. Buric, and G. Kusic, "Energy harvesting from mechanical vibrations using piezoelectric cantilever beams," in *Smart Structures and Materials 2006: Damping and Isolation*, 2006, vol. 6169: SPIE, pp. 81-92.

[14] H. A. Sodano, G. Park, and D. Inman, "Estimation of electric charge output for piezoelectric energy harvesting," *Strain,* vol. 40, no. 2, pp. 49-58, 2004.

[15] S. Jiang, X. Li, S. Guo, Y. Hu, J. Yang, and Q. Jiang, "Performance of a piezoelectric bimorph for scavenging vibration energy," *Smart materials and structures,* vol. 14, no. 4, p. 769, 2005.

[16] S. Roundy and Y. Zhang, "Toward self-tuning adaptive vibration-based microgenerators," in *Smart structures, devices, and systems II*, 2005, vol. 5649: SPIE, pp. 373-384.

[17] S. Roundy, P. K. Wright, and J. Rabaey, "A study of low level vibrations as a power source for wireless sensor nodes," *Computer communications,* vol. 26, no. 11, pp. 1131-1144, 2003.

[18] M. Safaei, H. A. Sodano, and S. R. Anton, "A review of energy harvesting using piezoelectric materials: state-of-the-art a decade later (2008–2018)," *Smart Materials and Structures,* vol. 28, no. 11, p. 113001, 2019.

[19] E. Lefeuvre, A. Badel, C. Richard, and D. Guyomar, "Piezoelectric energy harvesting device optimization by synchronous electric charge extraction," *Journal of intelligent material systems and structures,* vol. 16, no. 10, pp. 865-876, 2005.

[20] D. Guyomar, A. Badel, E. Lefeuvre, and C. Richard, "Toward energy harvesting using active materials and conversion improvement by nonlinear processing," *IEEE transactions on ultrasonics, ferroelectrics, and frequency control,* vol. 52, no. 4, pp. 584-595, 2005.

[21] A. Badel, D. Guyomar, E. Lefeuvre, and C. Richard, "Efficiency enhancement of a piezoelectric energy harvesting device in pulsed operation by synchronous charge inversion," *Journal of Intelligent Material Systems and Structures,* vol. 16, no. 10, pp. 889-901, 2005.

[22] E. Lefeuvre, A. Badel, C. Richard, and D. Guyomar, "High-performance piezoelectric vibration energy reclamation," in *Smart Structures and Materials 2004: Smart Structures and Integrated Systems*, 2004, vol. 5390: SPIE, pp. 379-387.

[23] P. C.-P. Chao, "Energy harvesting electronics for vibratory devices in self-powered sensors," *IEEE Sensors Journal*, vol. 11, no. 12, pp. 3106-3121, 2011.

[24] S. M. Hoseyni, M. ŞİMŞEk, A. Aghakhani, E. Lefeuvre, and I. Basdogan, "Multimodal piezoelectric energy harvesting on a thin plate integrated with SSHI circuit: an analytical and experimental study," *Smart Materials and Structures*, 2023. [Online]. Available: http://iopscience.iop.org/article/10.1088/1361-665X/ace9a0.

[25] Y. Shu, I. Lien, W. Wu, and S. Shiu, "Comparisons between parallel-and series-SSHI interfaces adopted by piezoelectric energy harvesting systems," in *Active and Passive Smart Structures and Integrated Systems 2009*, 2009, vol. 7288: SPIE, pp. 117-128.

[26] I. Lien, Y. Shu, W. Wu, S. Shiu, and H. Lin, "Revisit of series-SSHI with comparisons to other interfacing circuits in piezoelectric energy harvesting," *Smart Materials and Structures*, vol. 19, no. 12, p. 125009, 2010.

[27] H. Lin, P. Wu, I. Lien, and Y. Shu, "Analysis of an array of piezoelectric energy harvesters connected in series," *Smart Materials and Structures*, vol. 22, no. 9, p. 094026, 2013.

[28] D. Wu, D. Guyomar, and C. Richard, "A new global approach using a network of piezoelectric elements and energy redistribution for enhanced vibration damping of smart structure," in *Active and Passive Smart Structures and Integrated Systems 2013*, 2013, vol. 8688: SPIE, pp. 251-265.

[29] Y. Li, D. Guyomar, and C. Richard, "Influence of the topology for a networked SSHI piezoelectric harvesting configuration," in *Active and Passive Smart Structures and Integrated Systems 2013*, 2013, vol. 8688: SPIE, pp. 43-57.

[30] Y. Jeon, R. Sood, J.-H. Jeong, and S.-G. Kim, "MEMS power generator with transverse mode thin film PZT," *Sensors and Actuators A: Physical*, vol. 122, no. 1, pp. 16-22, 2005.

[31] F. Hua-Bin *et al.*, "A MEMS-based piezoelectric power generator for low frequency vibration energy harvesting," *Chinese Physics Letters*, vol. 23, no. 3, p. 732, 2006.

[32] C. Williams and R. B. Yates, "Analysis of a micro-electric generator for microsystems," *sensors and actuators A: Physical,* vol. 52, no. 1-3, pp. 8-11, 1996.

[33] N. E. Dutoit, B. L. Wardle, and S.-G. Kim, "Design considerations for MEMS-scale piezoelectric mechanical vibration energy harvesters," *Integrated ferroelectrics,* vol. 71, no. 1, pp. 121-160, 2005.

[34] A. Erturk and D. J. Inman, "On mechanical modeling of cantilevered piezoelectric vibration energy harvesters," *Journal of intelligent material systems and structures,* vol. 19, no. 11, pp. 1311-1325, 2008.

[35] S. Roundy, P. K. Wright, and J. M. Rabaey, "Energy scavenging for wireless sensor networks," in *Norwell*: Springer, 2003, pp. 45-47.

[36] L. Meirovitch, *Fundamentals of vibrations*. Waveland Press, 2010.

[37] N. W. Hagood, W. H. Chung, and A. Von Flotow, "Modelling of piezoelectric actuator dynamics for active structural control," *Journal of intelligent material systems and structures,* vol. 1, no. 3, pp. 327-354, 1990.

[38] F. Lu, H. P. Lee, and S. P. Lim, "Modeling and analysis of micro piezoelectric power generators for micro-electromechanical-systems applications," *Smart materials and structures,* vol. 13, no. 1, p. 57, 2003.

[39] S.-N. Chen, G.-J. Wang, and M.-C. Chien, "Analytical modeling of piezoelectric vibration-induced micro power generator," *Mechatronics,* vol. 16, no. 7, pp. 379-387, 2006.

[40] J. Lin, X. Wu, T. Ren, and L. Liu, "Modeling and simulation of piezoelectric MEMS energy harvesting device," *Integrated Ferroelectrics,* vol. 95, no. 1, pp. 128-141, 2007.

[41] A. Erturk and D. J. Inman, "Issues in mathematical modeling of piezoelectric energy harvesters," *Smart Materials and Structures,* vol. 17, no. 6, p. 065016, 2008.

[42] A. Erturk and D. J. Inman, "A distributed parameter electromechanical model for cantilevered piezoelectric energy harvesters," *Journal of vibration and acoustics,* vol. 130, no. 4, 2008.

[43] C. D. M. Junior, A. Erturk, and D. J. Inman, "An electromechanical finite element model for piezoelectric energy harvester plates," *Journal of Sound and Vibration,* vol. 327, no. 1-2, pp. 9-25, 2009.

[44] C. J. Rupp, A. Evgrafov, K. Maute, and M. L. Dunn, "Design of piezoelectric energy harvesting systems: a topology optimization approach based on multilayer plates and shells," *Journal of Intelligent Material Systems and Structures,* vol. 20, no. 16, pp. 1923-1939, 2009.

[45] A. Erturk, "Piezoelectric energy harvesting for civil infrastructure system applications: Moving loads and surface strain fluctuations," *Journal of Intelligent Material systems and structures,* vol. 22, no. 17, pp. 1959-1973, 2011.

[46] U. Aridogan, I. Basdogan, and A. Erturk, "Analytical modeling and experimental validation of a structurally integrated piezoelectric energy harvester on a thin plate," *Smart Materials and Structures,* vol. 23, no. 4, p. 045039, 2014.

[47] U. Aridogan, I. Basdogan, and A. Erturk, "Multiple patch–based broadband piezoelectric energy harvesting on plate-based structures," *Journal of Intelligent Material Systems and Structures,* vol. 25, no. 14, pp. 1664-1680, 2014.

[48] S. Roundy and P. K. Wright, "A piezoelectric vibration based generator for wireless electronics," *Smart Materials and structures,* vol. 13, no. 5, p. 1131, 2004.

[49] Y. S. Cho, Y. E. Pak, C. S. Han, and S. K. Ha, "Five-port equivalent electric circuit of piezoelectric bimorph beam," *Sensors and Actuators A: Physical,* vol. 84, no. 1-2, pp. 140-148, 2000.

[50] N. G. Elvin and A. A. Elvin, "A general equivalent circuit model for piezoelectric generators," *Journal of Intelligent Material Systems and Structures,* vol. 20, no. 1, pp. 3-9, 2009.

[51] Y. Yang and L. Tang, "Equivalent circuit modeling of piezoelectric energy harvesters," *Journal of intelligent material systems and structures,* vol. 20, no. 18, pp. 2223-2235, 2009.

[52] B. Bayik, A. Aghakhani, I. Basdogan, and A. Erturk, "Equivalent circuit modeling of a piezo-patch energy harvester on a thin plate with AC–DC conversion," *Smart Materials and Structures,* vol. 25, no. 5, p. 055015, 2016.

[53] A. Aghakhani and I. Basdogan, "Equivalent impedance electroelastic modeling of multiple piezo-patch energy harvesters on a thin plate with AC–DC conversion," *IEEE/ASME Transactions on Mechatronics,* vol. 22, no. 4, pp. 1575-1584, 2017.

[54] U. Aridogan, I. Basdogan, and A. Erturk, "Random vibration energy harvesting on thin plates using multiple piezopatches," *Journal of Intelligent Material Systems and Structures,* vol. 27, no. 20, pp. 2744-2756, 2016.

[55] G. K. Ottman, H. F. Hofmann, A. C. Bhatt, and G. A. Lesieutre, "Adaptive piezoelectric energy harvesting circuit for wireless remote power supply," *IEEE Transactions on power electronics*, vol. 17, no. 5, pp. 669-676, 2002.

[56] Y. Cai, K. Zhang, Z. Ye, C. Liu, K. Lu, and L. Wang, "Influence of temperature on the natural vibration characteristics of simply supported reinforced concrete beam," *Sensors*, vol. 21, no. 12, p. 4242, 2021.